

**Ice Crystal Multiplication in Convective Elements of Winter
Orographic Clouds**

By

Larry Vardiman

Department of Atmospheric Science
Colorado State University
Fort Collins, Colorado



**Department of
Atmospheric Science**

Paper No. 191

ICE CRYSTAL MULTIPLICATION IN CONVECTIVE ELEMENTS
OF WINTER OROGRAPHIC CLOUDS

by
LARRY VARDIMAN

This report was prepared with support provided by
National Science Foundation Grants
GA-26401 and GI-31460
Principal Investigator, Lewis O. Grant

Department of Atmospheric Science
Colorado State University
Fort Collins, Colorado

July 1972

Atmospheric Science Paper No. 191

ABSTRACT OF THESIS

ICE CRYSTAL MULTIPLICATION IN CONVECTIVE ELEMENTS OF WINTER OROGRAPHIC CLOUDS

This paper presents the results of a study of four winter orographic storms which contained precipitation cells, apparently convective in nature, and exhibited varying degrees of ice-crystal multiplication. Ice crystal-ice nuclei ratios in the cells were computed and studied in relation to cloud-top temperature.

For all crystal types, including regulars, irregulars, and fragments, the ratio of ice crystals to ice nuclei exhibited a trend to higher values at warmer temperatures. The line of best fit for the ratio of all ice crystals to ice nuclei versus cloud-top temperature predicts a ratio of one at a cloud-top temperature of -30°C . At the warm end, the ratio reaches a value greater than 10^4 at -14°C .

Similar curves for regular crystals, irregular crystals, and fragments, individually, showed nearly the same trend but had lower values. The curve for irregular crystals had a slightly reduced slope from the other types of crystals, indicating that irregular crystals constitute a greater fraction of the total concentration of crystals at colder temperatures.

The mechanism responsible for the ice-crystal multiplication, indicated in the study, is hypothesized to be mechanical fracturing of fragile dendritic crystals. One of the four storms studied had extremely low wind conditions which reduced the likelihood that the high concentrations of fragments observed during cell passage came from any other source but the cloud.

If this mechanism is responsible for the ice crystal-ice nuclei ratios observed, then clouds which contain dendritic-type crystals have a dramatically favorable region for ice-crystal multiplication. Seeding of convective clouds to increase precipitation will be less effective, as will other storm systems which contain convective cells.

Larry Vardiman
Department of Atmospheric Science
Colorado State University
Fort Collins, Colorado
July 1972

ACKNOWLEDGEMENTS

The author wishes to express his appreciation to Professor Lewis O. Grant for his guidance during the period of this study. He is also grateful to Drs. Charles Knight and Paul W. Mielke for their helpful suggestions. Mr. Dave Blancher is appreciated for his part in programming for the data analysis. He is grateful to his wife for her sustained devotion and particularly to God who created the beautiful ice crystals around which this study was centered.

This research was primarily supported by the Atmospheric Sciences Section, National Science Foundation, under Grants GA-26401 and GI-31460.

The material presented in this report is taken from a thesis by the author submitted as partial fulfillment of the degree of Master of Science at Colorado State University.

TABLE OF CONTENTS

<u>Section</u>	<u>Page</u>
ABSTRACT OF THESIS	iii
ACKNOWLEDGEMENTS	v
LIST OF TABLES	viii
LIST OF FIGURES	ix
INTRODUCTION	1
General Statement	1
Background	2
Objectives	4
THEORY	5
Ice-Nuclei Concentrations	5
Ice-Crystal Concentrations and Shapes	7
Ice-Crystal Fragility	9
PROCEDURE	13
General Procedure	13
Ice-Nuclei Concentrations	13
Ice-Crystal Concentrations	15
Convective-Cell Identification	16
FACILITIES AND DATA SOURCES	18
Bigg-Warner Expansion Chamber	18
Continuous Formvar Replicator	18
Radar	27
Temperature Soundings	27
Description of Orographic Storms	30
RESULTS	32
DISCUSSION OF RESULTS	39
Error Analysis	39
Scatter in the Data	42
Ice-Crystal-Multiplication Hypothesis	43
Impact on Weather Modification	48
SUMMARY AND RECOMMENDATIONS	50
REFERENCES	52

TABLE OF CONTENTS (Continued)

<u>Section</u>	<u>Page</u>
APPENDIX A	54
Ice-Crystal Classification	54
APPENDIX B	59
Fall-Velocity Equations	59
Crystal Concentrations	63
APPENDIX C	67
Trajectory Model	67
APPENDIX D	73
Data	73

LIST OF TABLES

Table	Page
1. Variation of Crystal Habit with Temperature	8
2. Key to Numbers in Figure 5	21
3. Extreme Errors in Ice Crystal-Ice Nuclei Ratios	40
A1. Crystal Classifications	55
A2. Crystal Classifications	56
A3. Measurable Crystal Dimensions	58
B1. Fall-Velocity Equations	60
B2. Example of Output from Crystal-Classification Program	64
D1. Summary of Data	74

LIST OF FIGURES

Figure	Page
1. Average Global and Climax Ice-Nuclei Spectra	6
2. Variation of Crystal Habit with Temperature and Supersaturation..	8
3. Theoretical Distribution of Ice Crystal-Ice Nuclei Ratio Versus Cloud-Top Temperature	12
4. Operation of Bigg-Warner Ice Nuclei Chamber	19
5. Mean Dependence of Ice-Nuclei Concentration on Activation Temperature for Various Counters	20
6. Operation of Continuous Formvar Replicator	23
7. Concentrations of Fragments, Irregulars, and Total Crystals Versus Time on February 14, 1969	24
8. Crystal Fragment Observed During Passage of Cell #20 on February 14, 1969	25
9. Crystal Fragment Observed During Passage of Cell #20 on February 14, 1969	25
10. Crystal Fragment Observed During Passage of Cell #20 on February 14, 1969	26
11. Radar Observation Site on Chalk Mountain Near Climax, Colorado..	28
12. Comparison of Interpolated Sounding to Actual Sounding at Climax, Colorado	29
13. Ratio of Regular Ice Crystals to Ice Nuclei Versus Cloud-Top Temperature	33
14. Ratio of Irregular Ice Crystals to Ice Nuclei Versus Cloud-Top Temperature	34
15. Ratio of Ice-Crystal Fragments to Ice Nuclei Versus Cloud-Top Temperature	35
16. Ratio of Total Ice Crystals to Ice Nuclei Versus Cloud-Top Temperature	36
17. Composite Plot of Ice-Crystal to Ice-Nuclei Ratios Versus Cloud-Top Temperature	37
18. Residual of IC/IN Ratio from the Temperature Regression Shown in Fig. 16 for total Crystals Versus the 500-mb. Wind Speed	44

LIST OF FIGURES (Continued)

Figure	Page
19. Example of a Convective Element Embedded in the General Orographic Cloud on March 30, 1972	46
B1. Computer Program Flow Chart	66
C1. Geometry of Radar Beam and Ice-Crystal Trajectories	68
C2. Ice-Crystal Delay Time from the First Observation of the Cloud on Radar to the Entrance of Crystals into the Replicator	71
D1. Synoptic Maps for January 31, 1968	75
D2. Synoptic Maps for April 18, 1968	76
D3. Synoptic Maps for January 25, 1969	77
D4. Synoptic Maps for February 14, 1969	78
D5. Temperature Sounding and Winds for Climax on January 31, 1968	79
D6. Temperature Sounding and Winds for Climax on April 18, 1968	79
D7. Temperature Sounding and Winds for Climax on January 25, 1969	80
D8. Temperature Sounding and Winds for Climax on February 14, 1969	80
D9. Ice-Nuclei Spectrum for January 31, 1968	81
D10. Ice-Nuclei Spectrum for April 18, 1968	82
D11. Ice-Nuclei Spectrum for January 25, 1969	83
D12. Ice-Nuclei Spectrum for February 14, 1969	84
D13. Ice-Crystal Variation with Time for January 31, 1968	85
D14. Ice-Crystal Variation with Time for April 18, 1968	86
D15. Ice-Crystal Variation with Time for January 25, 1969	87
D16. Ice-Crystal Variation with Time for February 14, 1969	88

INTRODUCTION

General Statement

Seeding of both orographic and convective clouds to increase precipitation is based on the assumption that additional ice crystals are required to convert the liquid water, which natural concentrations of ice crystals have not utilized, to large ice particles which can reach the ground. Ice-crystal concentrations that would correspond to observed natural concentrations of ice nuclei would frequently be insufficient to utilize all available supercooled cloud water. There is, however, increasing evidence that, at least in some clouds, ice-crystal concentrations far exceed those to be expected from observed ice-nuclei concentrations. Some investigators would argue that this so-called "ice-crystal multiplication" is not caused by abnormally high concentrations of ice crystals above that expected by activation of natural ice nuclei, but rather by the inability of the current ice-nuclei counters to measure the concentration of ice nuclei which a cloud activates. The variability in measurements among different ice-nuclei counters produces a feeling of uncertainty in the reliability of ice nuclei counters in general, but to date, no systematic error in ice nuclei measurements which would explain the observed trend in ice crystal-ice nuclei ratios with temperature has been reported. Therefore, the need for investigation of ice-crystal multiplication and its effect on weather modification has not been eliminated. In particular, there is evidence that ice-crystal multiplication is occurring during periods of orographic storms, and an investigation of the small-scale structure of orographic clouds is needed.

Background

For better than fifteen years the opinion has been held that some clouds contain more ice crystals than can be accounted for by the presumed concentration of heterogeneous ice-forming nuclei active at the temperature of the clouds. Mason (1955) pointed out the apparent necessity for the secondary production of ice nuclei during the steady release of snow from layer-cloud systems. He showed that in order to supply one nucleus per crystal, the air entering the cloud base would have to contain nucleus concentrations $10^2 - 10^3$ times higher than are normally measured at -15°C , and suggested that the additional nuclei are produced by small splinters being torn off the fragile dendritic crystals and that these can then serve as nuclei for new crystals.

As improved methods of cloud sampling became available, instances of ice-crystal multiplication were reasonably well documented. The disparity between ice-crystal and ice-nuclei concentrations appears to be the greatest in convective and maritime clouds and least in stratiform clouds. Koenig (1963, 1968) and Braham (1964) reported that summer continental cumulus clouds in Missouri, with cloud-top temperatures warmer than -10°C , often contain ice particles in concentrations which are several orders of magnitude greater than would be expected from ice-nucleus measurements. Mossop (1967, 1968) reported that maritime clouds also have large disparities between ice-crystal and ice-nuclei concentrations but evidently do not universally have the properties necessary for ice-crystal multiplication. He observed that only one of several apparently similar turrets rising from a stratiform deck contained abnormally high ice-crystal concentrations on the order of $10^3 - 10^4$ greater than expected.

Hobbs (1969) and Auer, et al. (1969) found that the differences in ice-crystal and ice-nuclei concentrations tend to be greater at warmer cloud temperatures. Hobbs determined that the ratio of ice crystals to ice nuclei becomes one at a cloud-top temperature of -26°C . Auer, et al., found a similar slope but the ratios were somewhat greater at equalivalent cloud temperatures. Thus, at -25°C their ratio was still 17, versus nearly 1 for Hobbs.

Hindman (1967) studied winter, orographic storms near Climax, Colorado to determine if ice-crystal multiplication was occurring. He found that "the average snow crystal and ice-nuclei concentrations measured at the ground were approximately equal for the same crystal formation temperatures". In his study, Hindman considered only regular crystals which formed at temperatures warmer than -20°C and averaged their concentrations over entire storms. He then compared these average concentrations with average ice-nuclei concentrations determined by a Bigg-Warner chamber and multiplied by a correction factor of 3.5. Since Hindman's study, the correction factor was found to be unnecessary and therefore his ratio of ice crystals to ice nuclei are low by a factor of 3.5. In addition, by averaging over an entire storm, any effect of ice-crystal multiplication which has occurred during short periods of the storm would have been diluted considerably, depending upon the extent and duration of the periods of ice-crystal multiplication. The neglect of irregular crystals, which comprise more than 50% of the ice crystals in most storms at Climax, also eliminates an important contribution to the total concentration of ice crystals.

Objectives

Research is in progress at Colorado State University to define ice-crystal multiplication in winter orographic clouds located over the continental divide near Climax, Colorado. Evidence of ice-crystal fragmentation associated with peaks in precipitation intensity led to the study of multiplication mechanisms in convective cells.

The purposes of this study are to:

1. Compare ice-crystal and ice-nuclei concentrations in convective cells of winter, orographic storms as a function of cloud-top temperature.
2. Discuss the results in terms of other research and propose an hypothesis to explain the effect.

THEORY

Ice-Nuclei Concentrations

At cloud temperatures warmer than about -40°C with no artificial cloud seeding, no natural seeding by upper-level clouds, and no ice-crystal multiplication within a cloud; ice crystals which form in a cloud must be nucleated by natural concentrations of heterogenous ice-forming nuclei. Not all natural ice nuclei are activated at the same temperature but are effective at varying temperatures depending upon size and composition. Fletcher (1962) has determined an average ice-nuclei spectrum which is representative of a large portion of the globe. Figure 1 shows Fletcher's spectrum. In regions where artificial sources of ice nuclei are present, or where ice nuclei have been depleted, this spectrum will differ considerably. On a day-to-day basis the ice-nuclei spectrum has also been found to change.

Chappell (1970) determined an average ice-nuclei spectrum for the area of the continental divide near Climax, Colorado. His spectrum, also shown in Fig. 1, exhibits a reduced slope from Fletcher's. The reduced slope predicts greater concentrations of ice nuclei than Fletcher's spectrum at temperatures warmer than about -19°C and lower concentrations at temperatures colder than -19°C . For Fletcher's concentration of activated ice nuclei to change by a factor of ten the temperature must change by 4C° , while Chappell's spectrum requires that the temperature change by 5.3C° for the same effect.

Under natural conditions, concentrations of ice nuclei have been found to be reasonably constant with height in the lower atmosphere except in the presence of inversions. Therefore, the concentration

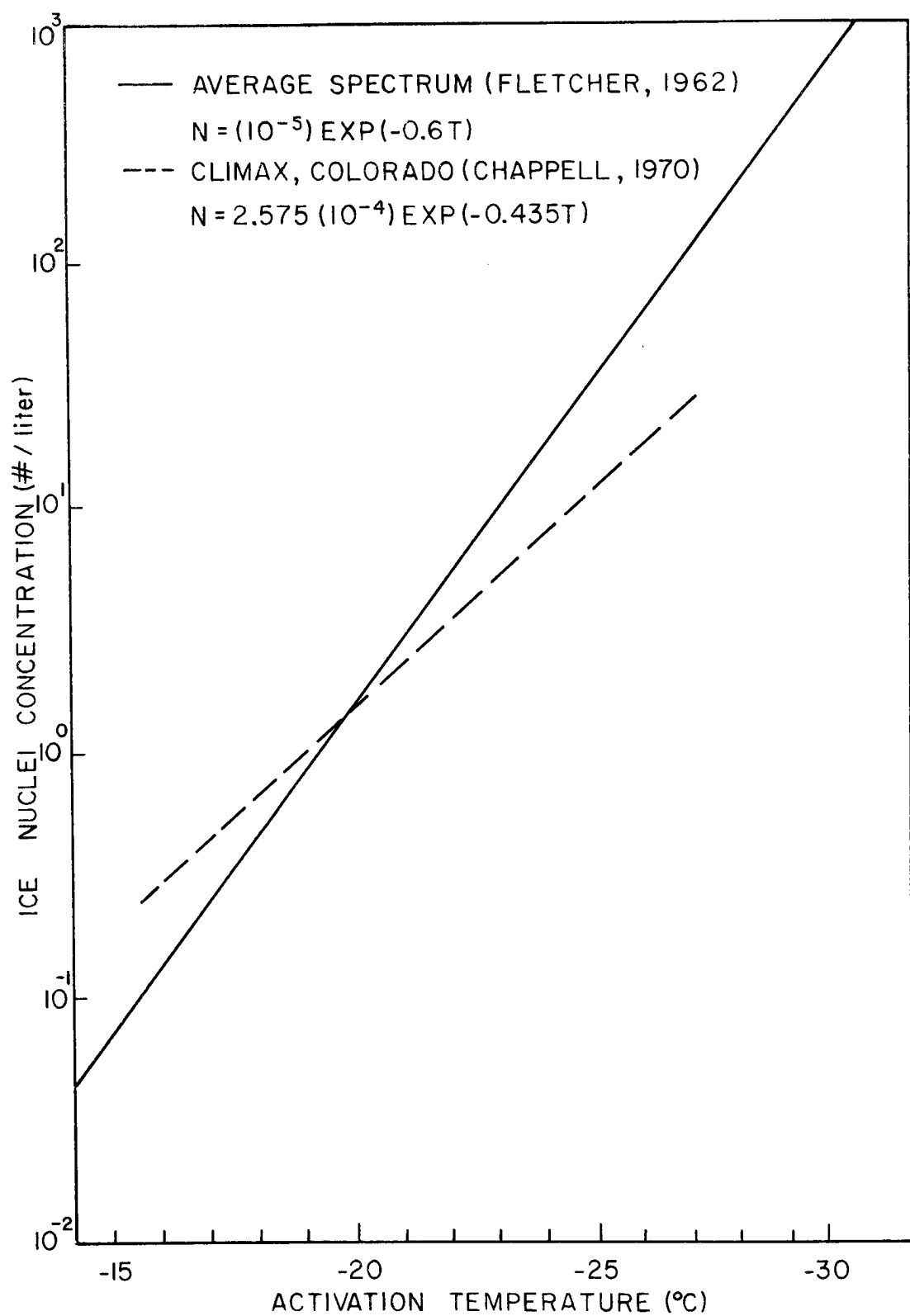


Fig. 1 Average Global and Climax Ice-Nuclei Spectra

of ice nuclei activated with height depends only upon the ice-nuclei spectrum.

Since temperature decreases with height in the atmosphere, the concentration of ice nuclei activated increases with altitude. With the exception of inversion conditions, the cloud top will be the coldest portion of the cloud and thereby will activate the largest numbers of ice nuclei.

Ice-Crystal Concentrations and Shapes

The concentration of ice crystals generated in a cloud by activation of heterogeneous ice nuclei should be the greatest at cloud top in accordance with the previous discussion. As these crystals grow and attain a fall velocity large enough to overcome the updraft in the cloud, they will descend into warmer regions of the cloud and grow in shapes determined by the temperature and supersaturation. Hallett and Mason (1958) have reported one of the latest in a series of investigations on the crystal habits of ice as a function of temperature and supersaturation. Their results are shown in Fig. 2 and Table 1. If a cloud has a cloud-top temperature of -20°C the crystals generated at the top will grow initially as plates. As they fall downward through the cloud they will form sectorlike extensions and then dendritic arms, if the supersaturation is great enough. The crystals will continue to change form until reaching the ground. For crystals which have made a single traverse through the cloud without complicated up and down motions, the temperature and humidity structure of the cloud can be estimated from the final form of the crystals.

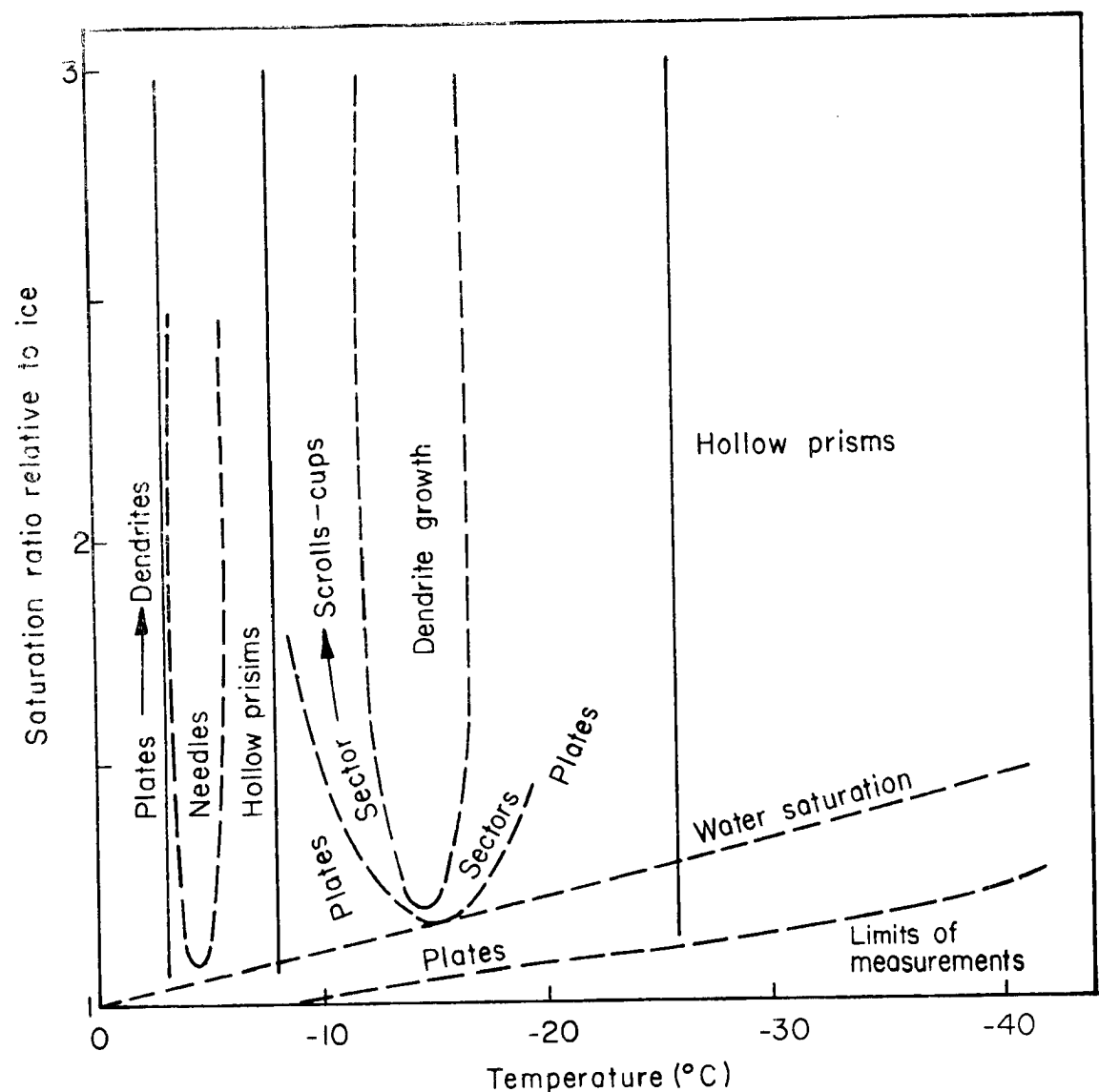


Fig. 2 Variation of Crystal Habit with Temperature and Supersaturation

TEMP. RANGE (°C)	CRYSTAL HABIT
0 to - 3	Thin Hexagonal Plates
- 3 to - 5	Needles
- 5 to - 8	Hollow Prisms
- 8 to -12	Hexagonal Plates
-12 to -16	Dendritic Crystals
-16 to -25	Plates
-25 to -50	Hollow Prisms

Table 1 Variation of Crystal Habit with Temperature

For a cloud with a warmer top a similar sequence occurs, but the central core of the crystal should indicate a different formation temperature. For example, a crystal which traversed a cloud whose top was -15°C should show dendritic growth in the center with sectorlike extensions and plates on the ends.

Ice-Crystal Fragility

A singular lack of information is evident regarding the strength of individual crystals of ice under impact conditions. The primary impetus for research into the mechanical properties of ice has been avalanche studies and glacier movements. Both of these areas require physical data on elastic properties and creep in ice, neither of which is suitable for short-period, inelastic collisions between crystals or small-scale turbulence in clouds. The author is attempting to obtain the necessary information from laboratory studies but these data are not available for this paper. A qualitative argument will be offered instead.

Assuming that the mechanical strength of ice is isotropic for inelastic processes, the factors which effect the structural strength of individual crystals are the moment arm through which fracturing forces act, and the cross-sectional area of the arm. Although elastic properties of ice have been shown to be fairly isotropic, inelastic properties may not be isotropic because of the layered structure of ice. However, there are no data on which to make a better assumption. Considering only moment arms and cross sections, the dendritic crystals which form near -15°C exhibit the weakest structure because of their long moment arms and small cross sections. At warmer and colder

temperatures from the dendritic region the crystals appear stronger. The plate crystals appear so strong that it would be difficult to imagine any process in the cloud which would have sufficient energy to fracture them. Intermediate between the dendritic region and the two plate regions at -12°C and -19°C are regions in which sector-like extensions grow. These sector-like extensions are shaped somewhat similarly to plates but are much thinner and could produce fragments for high-energy processes. The needle crystal which forms around -4°C also exhibits a weak structure. It has thin extensions on the ends which have small cross sections and are susceptible to fracturing.

The two temperature regions in which fracturing would most likely be expected then, would be centered around -4°C and -15°C , although the -15°C region is expected to be more important.

The question could reasonably be asked; would one expect fragmentation of ice crystals to affect the ice crystal-ice nuclei ratio for all clouds which are -15°C and colder if they contain a dendritic formation region? If the dendritic region does, in fact, contribute additional ice crystals because of fragmentation, one would expect to see a maximum ratio of ice crystals to ice nuclei for clouds with a cloud-top temperature of -15°C . At colder temperatures the ratio would decrease slowly to one at the point where the concentration of ice nuclei activated overweights the ice-multiplication process. For example, if the number of ice crystals produced at the -15°C level (about .2 crystals/liter) is multiplied by a factor of 10^3 , due to fragmentation, the total number of crystals convected up through the layer will be 200 crystals/liter. If the cloud-top temperature is -30°C , then the expected number of ice crystals produced by the

activation of ice nuclei at cloud top would also be about 200 crystal/liter. Then the total number of ice crystals one observes would be only twice that expected without the fragmentation process.

On the warm side of the -15°C region, one would expect the ratio of ice crystals to ice nuclei to fall off almost vertically towards warmer temperatures. This is due to the absence of any ice-crystal multiplication mechanism in the cloud.

If the -4°C region is also effective as a crystal generating region by fracturing, one would expect to see a similar trend with temperature, although probably not as great.

Figure 3 shows the theoretical distribution of the ice crystal-ice nuclei ratio versus cloud-top temperature if mechanical fracturing of fragile dendritic and needle-type crystals is the only mechanism responsible for ice-crystal multiplication. Absolute magnitudes of the ratios are probably not correct, but the relative importance of the needle and dendrite regions plus the general shape of the curves are the main thrust of Fig. 3.

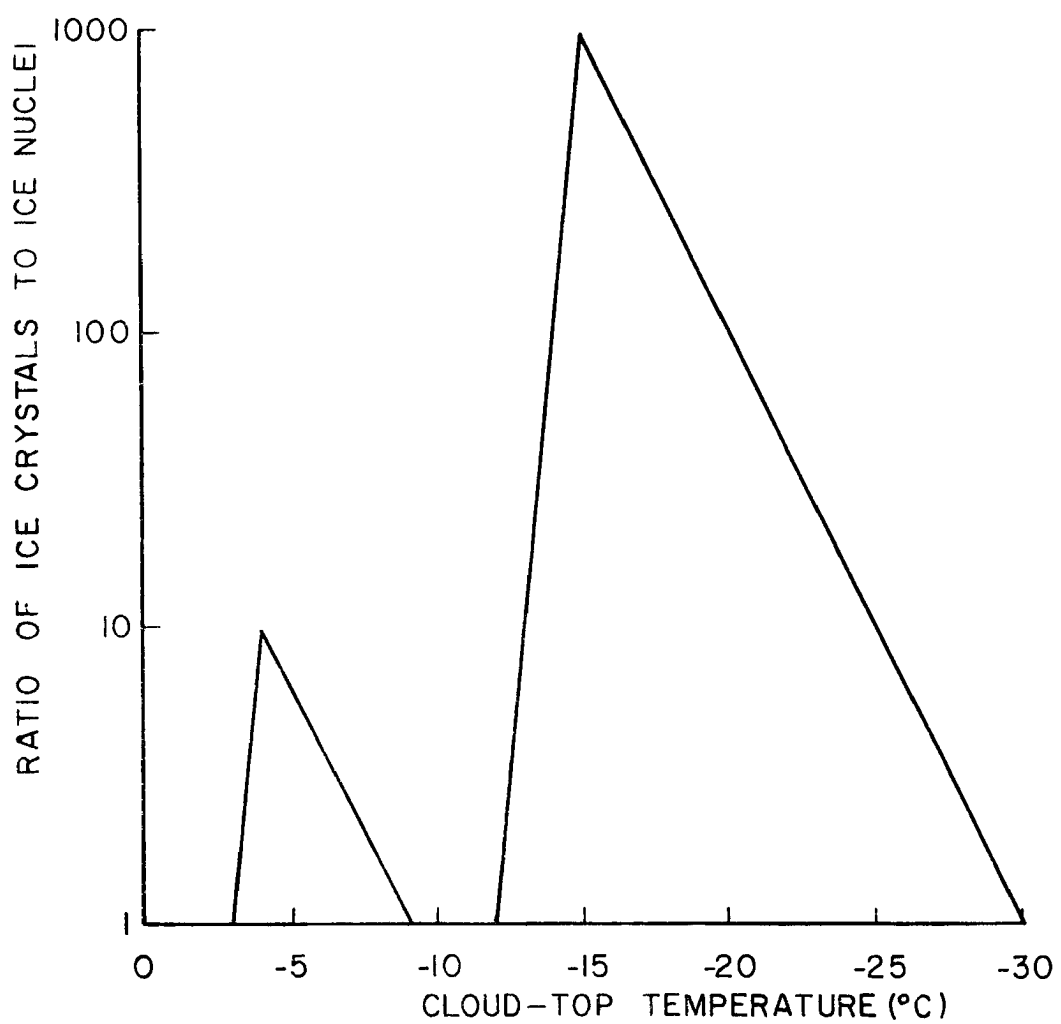


Fig. 3 Theoretical Distribution of Ice Crystal-Ice Nuclei Ratio Versus Cloud-Top Temperature

PROCEDURE

General Procedure

In this study, ice-crystal concentrations observed at the ground during passage of convective cells were compared to the estimated concentrations of ice nuclei which should have been activated at the top of the same cells. Concentrations of regular crystals, irregular crystals, fragments, and total crystals are included. It is assumed that the majority of the primary ice crystals are nucleated at the coldest cloud temperatures near cloud top and any additional ice crystals observed are due to an ice-multiplication process. Since the ice-nuclei measurements were made at the ground, it is also assumed that natural ice-nuclei concentrations are uniform with height.

Ice-Nuclei Concentrations

Ice-nuclei concentrations at cloud top were estimated by observing the heights of cloud top with radar, comparing the heights obtained to temperature soundings adjusted for space and time, and equating the ice-nuclei concentrations activated at cloud top to the ice-nuclei concentrations measured at the ground for the same temperature.

The radar used to observe cloud tops had a beam width of one degree and was inclined at an angle of $3^{\circ} 13'$ above the horizontal. The beam intersected the cloud tops at various ranges from the radar depending upon their height. The cloud top was determined for each cell by observing the maximum range at which the echo first appeared on the PPI scope as the cells moved toward the radar site. The maximum range at which an echo could be observed limited the heights of the

clouds which were studied. The highest cloud measured was one whose top reached to 6750 feet above the radar.

The cloud-top temperature was determined by comparing the cloud height to a sounding representative of the Climax area. The soundings for Climax were obtained by interpolating the soundings from Denver and Grand Junction. Weighting factors determined by the distances from Climax were used in the interpolation scheme as shown in the following equation.

$$T_{ci} = \frac{XT_{Gi} + YT_{Di}}{X + Y} = .38T_{Gi} + .62T_{Di} \quad (1)$$

where,

T_{ci} = Temperature at level i for Climax

T_{Gi} = Temperature at level i for Grand Junction

T_{Di} = Temperature at level i for Denver

X = Distance from Climax to Denver

Y = Distance from Climax to Grand Junction

In addition to the interpolation for distance, the soundings at Climax were then adjusted for variation with time. Soundings for 0800, 1100, and 1400 MST were obtained by linearly interpolating the 0500 and 1700 MST Climax soundings. These soundings were then applied to those portions of the storms studied to determine the cloud-top temperatures.

An ice-nuclei activation spectrum for each storm was plotted from the ice-nuclei measurements made at the ground at the High Altitude Observatory (HAO). Measurements were made with a Bigg-Warner Chamber

for activation temperatures ranging from -14°C to -28°C at intervals of 2°C . The number of measurements for each activation temperature in a storm varied from 1 to 12. During the period of a storm, all measurements at a given activation temperature were averaged and then plotted on semilog graph paper. The line of best fit through the data then determined the ice-nuclei activation spectrum.

The concentration of ice nuclei activated at the top of an individual cell was then obtained by "picking off" the concentration of ice nuclei from the spectrum effective at the cloud-top temperature.

Ice-Crystal Concentrations

Ice-crystal concentrations were calculated from the density of ice crystal replicas on strips of 35-mm film exposed during the storms. The ice-crystal replicator developed by Hindman and Rinker (1967) was positioned at HAO for three of the storms and on Chalk Mountain near the radar site for the other storm. In all four storms the surface winds observed were less than 5 knots and, for the majority of the period of study, were calm.

The replicator film was analyzed by projecting an image of the film onto a calibrated surface where crystal types and sizes were determined. The classification scheme used was that of Magono and Lee (1966) modified slightly to make computer calculations easier. The details of the classification scheme are shown in Appendix A. When the classification and sizing work was accomplished, the data were placed on computer cards which were, in turn, stored on magnetic tape.

A computer program was written to convert the crystal-density data to concentrations using the fall-velocity equations found experimentally

by Brown (1970). Fall-velocity equations for irregular crystals and fragments, which Brown did not consider, were derived from considerations of similarity to other crystals. The fall-velocity equations used in the program and a flow diagram are included in Appendix B. Included in the program was a sorting routine which reclassified all of the crystal types of the earlier classification into eight major groupings and twenty-eight sub-groupings. For this paper, the full resources of this classification scheme were not utilized, but future studies may rely heavily upon the calculations made available by this program. Only the four species of crystals - regular, irregular, fragments, and total crystals - were used to characterize the processes in the four storms studied.

An auxiliary program was formulated to plot the data after smoothing with a fifteen-minute running mean. These plots of ice-crystal concentration with time aided greatly in identifying which radar cell corresponded to a given peak in ice-crystal concentration.

The ice-crystal concentration for an individual cell was determined by averaging the peak concentration over a fifteen-minute period. Most peaks in crystal concentration due to cell passages were 30-40 minutes wide on the plot of concentration versus time. It was felt that a fifteen-minute average, although conservative, would best represent the maximum concentration of ice crystals in a cell over a significant portion of the cloud volume.

Convective-Cell Identification

One of the most apparent characteristics of both radar data and ice-crystal concentration data from orographic clouds over the

continental divide is its periodic nature. When one studies the features of both types of data, it becomes evident that convective activity of some nature must be embedded in the general orographic cloud during portions of its existence. It is not immediately apparent, however, which peak in ice-crystal concentration observed at the ground corresponds to a given radar cell.

A trajectory model was developed to aid in identifying where crystals originated which produced peaks in the concentration. The model considered the height of a cloud, the average fall velocity of the ice crystals, and the horizontal wind speed. When these parameters were put into the model, it provided a delay time which predicted when a peak in ice-crystal concentration could be expected on the ground after the appearance of a cell on the radar. Although the model was extremely crude, it provided quite reliable predictors when used in conjunction with characteristic signatures of the peaks in the ice-crystal concentration. A description of the model is given in Appendix C.

FACILITIES AND DATA SOURCES

Bigg-Warner Expansion Chamber

Ice-nuclei measurements were made with a Bigg-Warner expansion chamber positioned at HAO (See Fig. 4). No correction was made to the measurements in accordance with the results reported by the Second International Workshop on Condensation and Ice Nuclei (1971) held in 1970 in Fort Collins. Figure 5 shows the results of the workshop for the measurement of natural ice nuclei. The standard spectrum adopted for natural ice nuclei was an average between the measurements made by Gagin (5) and Otake (2). The Bigg-Warner chamber measurements taken by Reinking (11) at the workshop were completely within the bounds set by Gagin and Otake's data, although measurements made by Carnuth (10) with a similar instrument fell somewhat lower. The standard adopted at the workshop may not be identical to the concentration of ice nuclei that a cloud activates but, at this stage, there is little choice but to assume a reasonable standard and proceed. The main difference among ice-nuclei counters appears to be the relative values of ice nuclei measured rather than the slope of the spectra obtained. The magnitude of the effect observed in this paper depends upon the actual value of ice nuclei activated; but the trend with temperature, which is the more important aspect, depends upon the slope of the ice-nuclei spectra. Since the slope seems to agree reasonably well among most ice-nuclei counters, the trend seems to be assured.

Continuous Formvar Replicator

A continuous formvar replicator designed by Hindman and Rinker (1967) was used to obtain a record of ice-crystal production from the



Fig. 4 Operation of Bigg-Warner Ice-Nuclei Counter

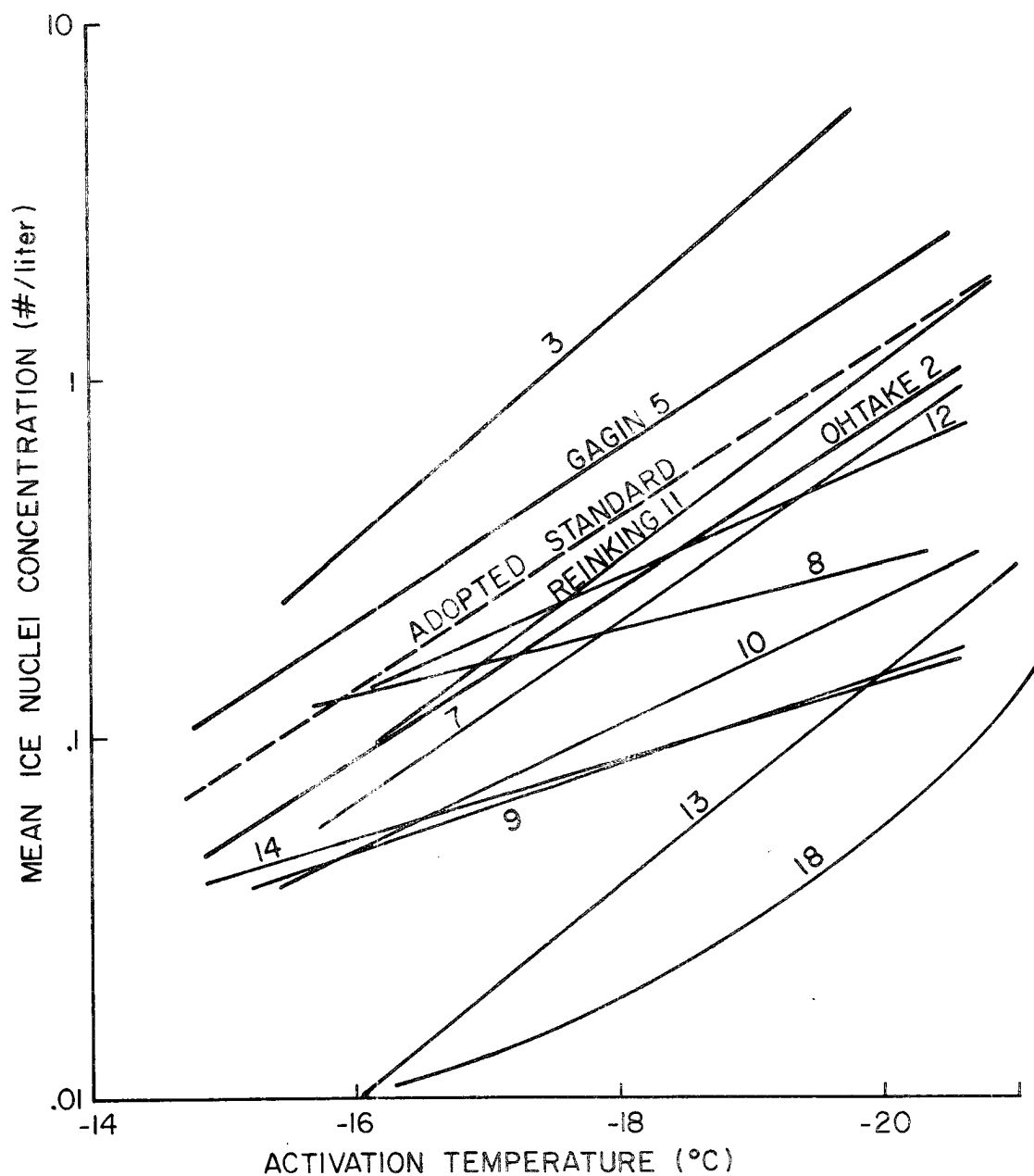


Fig. 5 Mean Dependence of Ice-Nuclei Concentration on Activation Temperature for Various Counters

KEY TO NOS. IN FIG. 5	MEASURING SYSTEM	OBSERVER
2	SETTLING-CLOUD CHAMBER	OHTAKE
3	GOETZ AEROSOL SPECTROMETER (100% R.H.)	GERBER
5	MEMBRANE FILTER	GAGIN
7	MEMBRANE FILTER	BIGG
8	MEMBRANE FILTER	VALI
9	MEMBRANE FILTER (DROPLET METHOD)	LANGER
10	RAPID EXPANSION COUNTER (B-W TYPE)	CARNUTH
11	RAPID EXPANSION COUNTER (B-W TYPE)	REINKING
12	RAPID EXPANSION COUNTER (CSU TYPE)	VARDIMAN
13	NCAR LONG-CONE ACOUSTIC COUNTER	LANGER
14	NCAR ACOUSTIC COUNTER	SCHNELL
18	DROPLET FREEZING	ROBERTSON

Table 2 Key to Numbers in Fig. 5

storms (See Fig. 6). A 4% solution of formvar in ethylene dichloride plus toluene was used in the replicator.

A detailed study of a storm on February 14, 1969, was made to determine if the crystal fragments frequently observed were produced in the cloud or by the replication technique. The wind conditions in this storm precluded the likelihood that crystal fragments had been advected to the replicator from trees or the surface. Figure 7 shows the concentrations of fragments, irregulars, and total ice crystals at HAO as a function of time on February 14, 1969. Cell #20 showed the highest concentration of fragments followed by lower concentrations with each succeeding cell. The concentration of irregular crystals between cells increased throughout the period, however. Figures 8, 9, and 10 show typical examples of crystal fragments observed. By far, the majority of fragments were like Fig. 9, but Figs. 8 and 10 were included to indicate the occurrence of fracturing and regrowth of the crystals before entering the replicator. Figure 8 is particularly interesting as it shows a crystal which had one branch broken off. The two nearest branches grew at an increased rate relative to the others because the missing branch changed the vapor diffusion field around the crystal. Figure 10 shows a crystal with regrowth after one branch was broken.

From this study, it was determined that the data obtained from the replicator reliably portrayed the actual ice-crystal distribution which falls from an orographic cloud. The occurrence of large concentrations of fragments coincident with cell passages, noted in this study, was largely responsible for the statistical evaluation reported in this paper.

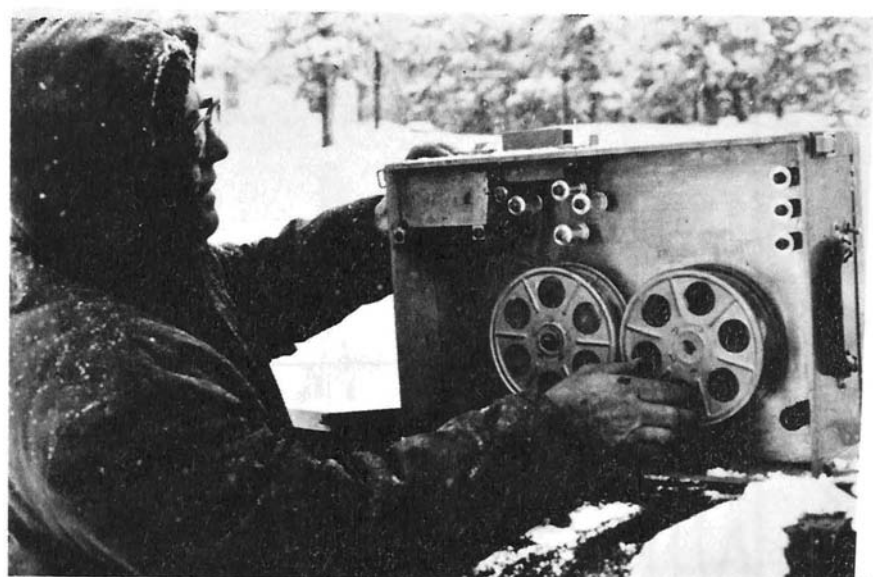


Fig. 6 Operation of Continuous Formvar Replicator

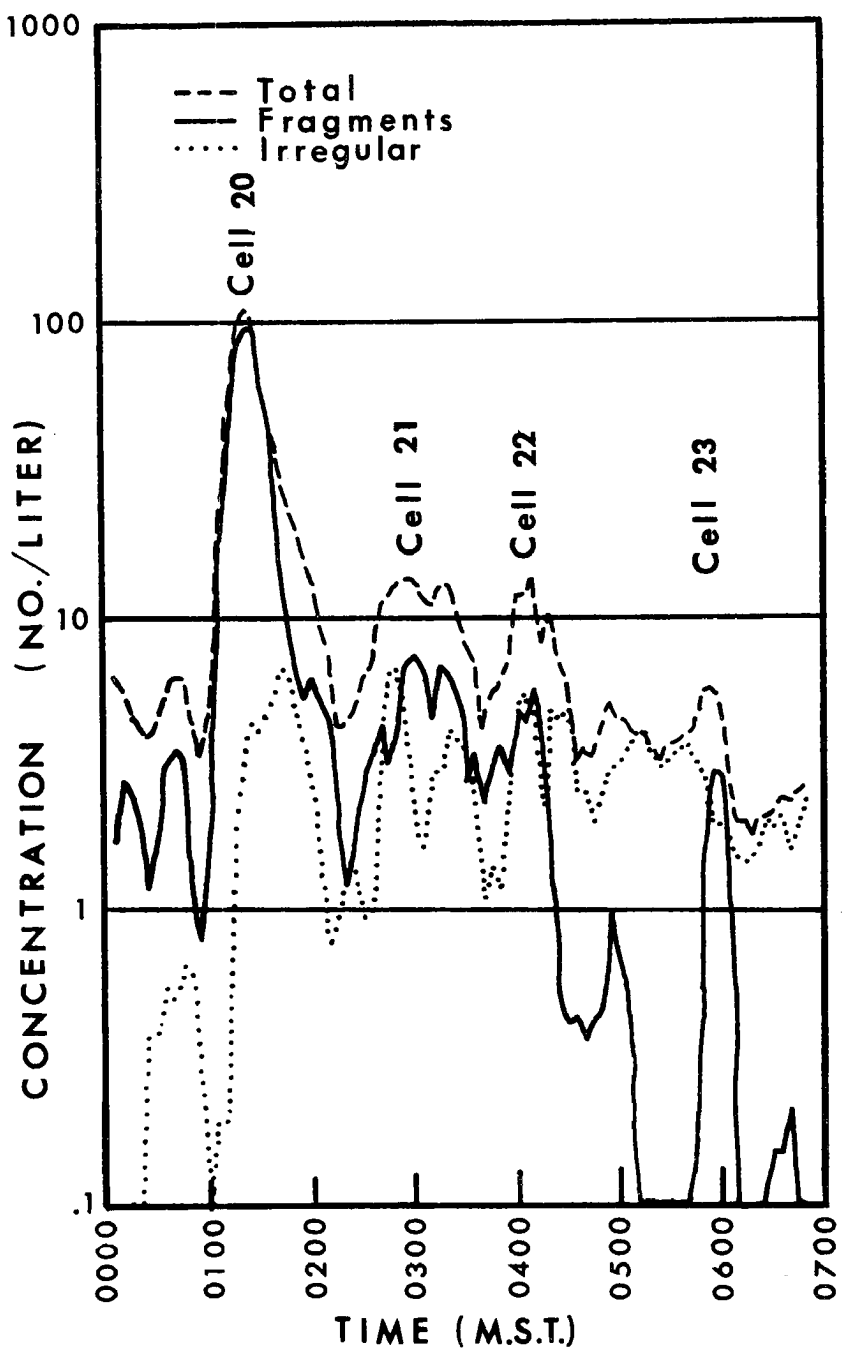


Fig. 7 Concentrations of Fragments, Irregulars, and Total Crystals Versus Time on February 14, 1969

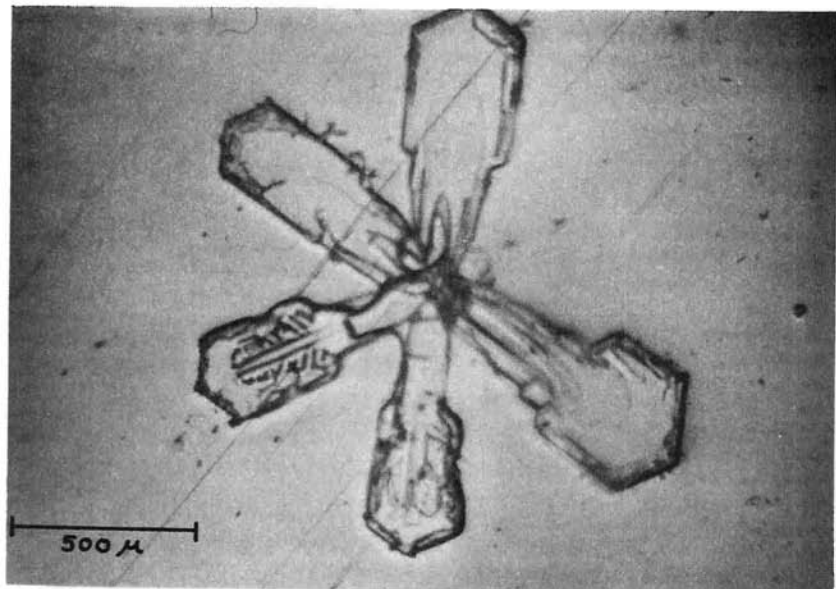


Fig. 8 Crystal Fragment Observed During Passage of Cell #20 on February 14, 1969

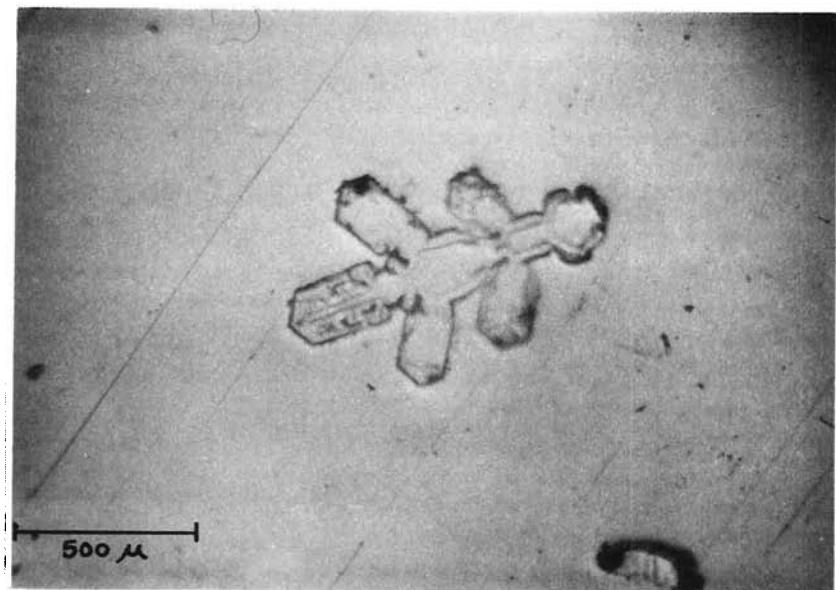


Fig. 9 Crystal Fragment Observed During Passage of Cell #20 on February 14, 1969

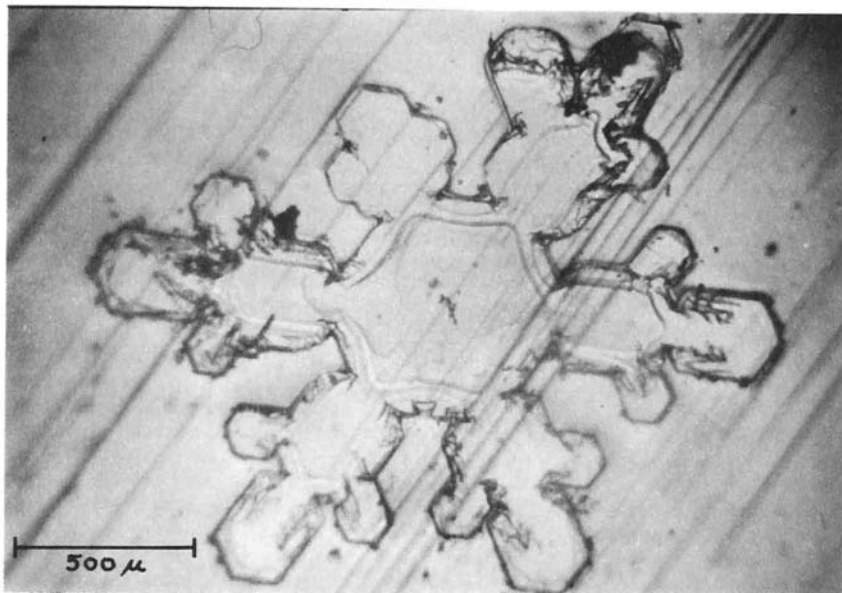


Fig. 10 Crystal Fragment Observed During Passage of
Cell #20 on February 14, 1969

Radar

An S0-12 M/N X-band radar was used to observe cloud tops. It was modified for a circular antenna and a plan position indicator (PPI). The radar has a beam width of one degree, which is equivalent to 2100 feet at 20 nautical miles, the maximum distance at which clouds were observed. The radar was positioned on top of Chalk Mountain near Climax, Colorado at an elevation of 12,000 feet (See Fig. 11).

In studying the characteristics of this radar in orographic storms, Furman (1967) found that "Convective activity is characterized by reflectivities stronger than those of the cloud in which it is embedded. This difference in reflectivity is caused by a higher concentration of larger particles". He found that attenuation was not a problem in orographic clouds. A primary source of error in this study was the determination of cloud top by radar, due to the uncertainty in the difference between radar tops and actual cloud tops. Less error is realized in measuring convective cloud tops than the general orographic tops because of the sharper gradients in ice crystal concentrations. Even a substantial error, however, does not affect the basic conclusions, as will be discussed later.

Temperature Soundings

The temperature soundings for Climax were obtained by interpolating the Denver and Grand Junction Soundings. For several of the storms a sounding was made from Climax which allowed comparison of actual temperatures with the interpolated soundings. Actual soundings at Climax were not frequent enough during the portions of the storms studied to allow their use exclusively. Figure 12 shows the good

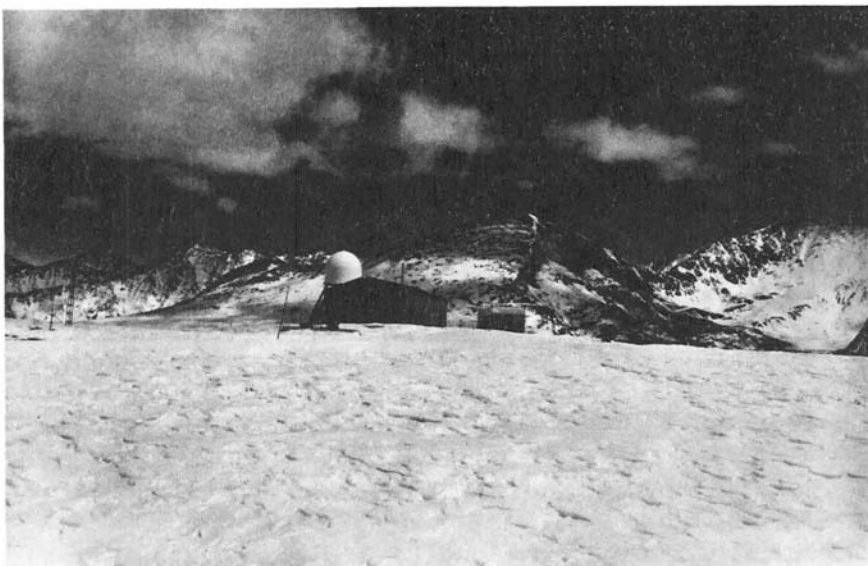


Fig. 11 Radar Observation Site on Chalk Mountain Near Climax, Colorado

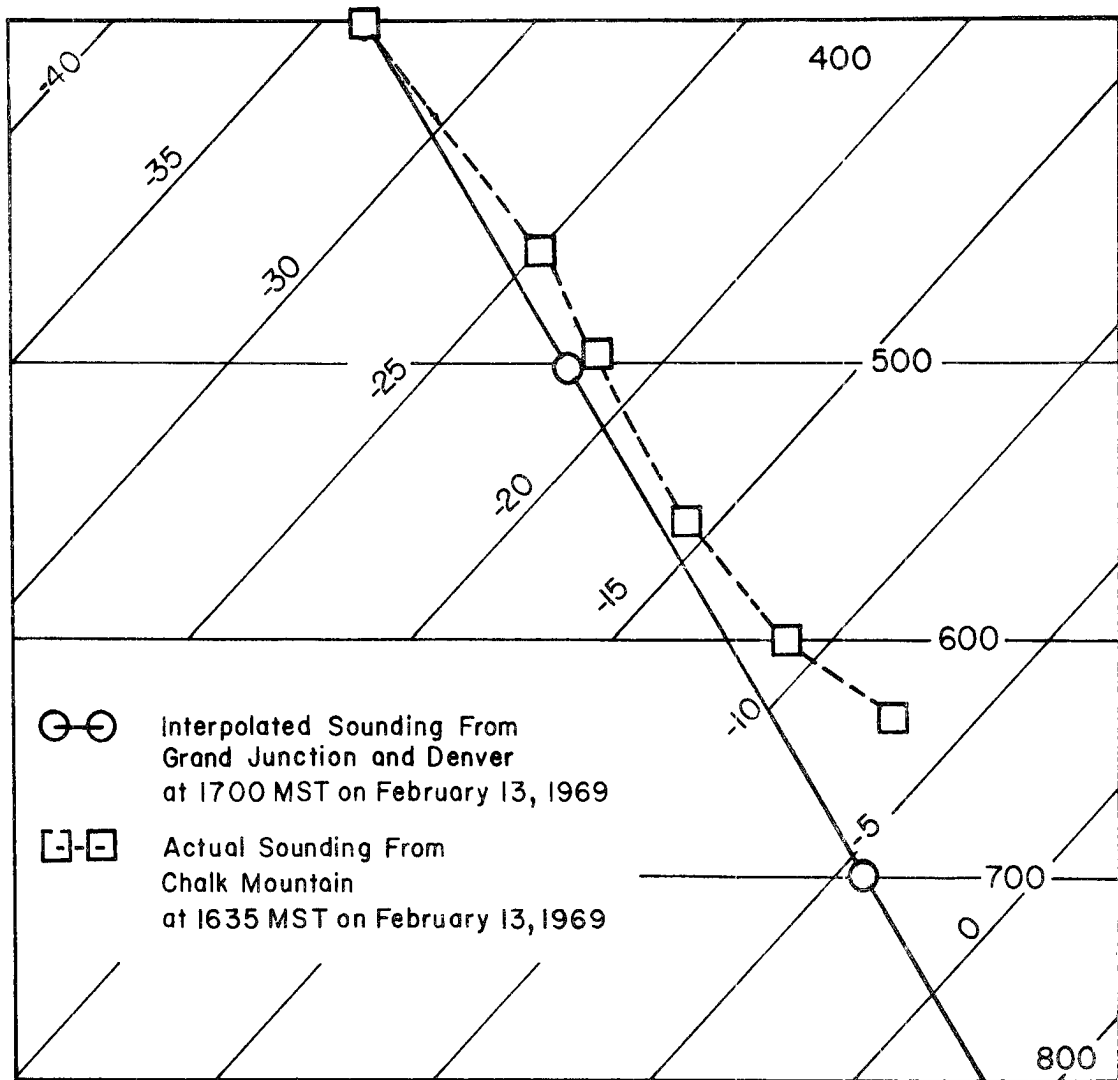


Fig. 12 Comparison of Interpolated Sounding to Actual Sounding
at Climax, Colorado

agreement between temperature soundings made at Climax and interpolated soundings during orographic storms. In most cases the soundings agreed quite well.

Description of Orographic Storms

Four winter orographic storms, two in 1968 and two in 1969, were studied. The following descriptions provide the important features of each storm. Ice-nuclei spectra, ice-crystal concentrations, temperature soundings, 500-mb maps, and surface maps for each storm are included in Appendix D.

January 31, 1968 - This storm can be characterized as a cold storm. The 500-mb. temperature averaged -25°C with winds of about 20 knots from WSW. Ice-nuclei concentrations averaged .8 per liter at an activation temperature of -20°C . Radar cloud tops extended to a maximum of 18,000 feet with the cloud-top temperatures ranging from -23.5°C to -26°C .

April 18, 1968 - The 500-mb. temperature in this storm averaged -23°C and the winds were about 20 knots from SSW. The ice-nuclei concentrations were about .6 per liter at an activation temperature of -20°C . Radar cloud tops reached a maximum of 18,000 feet and varied from -20.5°C to -22.5°C .

January 25, 1969 - This storm could be characterized as a warm storm with low ice-nuclei concentrations. The 500-mb. temperature averaged -18°C with winds as high as 50 knots from WNW. Ice-nuclei concentrations averaged .3 per liter for an activation temperature of -20°C .

Radar cloud tops reached a maximum of almost 19,000 feet and cloud-top temperatures varied from -17°C to -19.5°C .

February 14, 1969 - This storm was unique because of the wind conditions. The 500-mb. wind averaged about 10 knots from WSW and the surface wind was calm for nearly the entire period of the study. The 500-mb. temperature averaged -12°C but cloud tops were fairly low at 15,000-17,000 feet. Cloud-top temperatures varied from -16°C to -20.5°C . The ice-nuclei concentrations were .4 per liter at an activation temperature of -20°C .

RESULTS

Figures 13, 14, 15, and 16 are plots of the ratio of crystals observed at the ground to the concentration of ice nuclei which was estimated to have been activated at cloud top versus cloud-top temperature. Figure 17 is a composite plot of Figs. 13, 14, 15, and 16 without the data points.

A trend of greater ice crystal-ice nuclei ratios at warmer temperatures occurs for all crystal categories. This trend is somewhat surprising for regular crystals since regular crystals are normally assumed to have been nucleated and grown without interference from multiplication mechanisms. This trend in the regular crystals implies that some multiplication mechanism is providing additional crystals which grow and become indistinguishable from those which were nucleated and grew as primary crystals.

The difference in the slope for the irregular crystals shows the greater prevalence of irregulars at colder temperatures. According to this plot, at cloud-top temperatures of -27°C and colder, almost all of the ice crystals are irregular.

The curve corresponding to fragments exhibits a slightly greater slope compared to the irregulars. At warmer temperatures the percentage of fragments is greater, relative to the other crystal types, than at colder temperatures. This trend is in agreement with the conceptual curve shown in Fig. 3.

Since only one cell was warmer than -15°C , it is not possible to determine if the observed ratio would drop abruptly at cloud-top temperatures on the warm side of the dendritic region as it does in

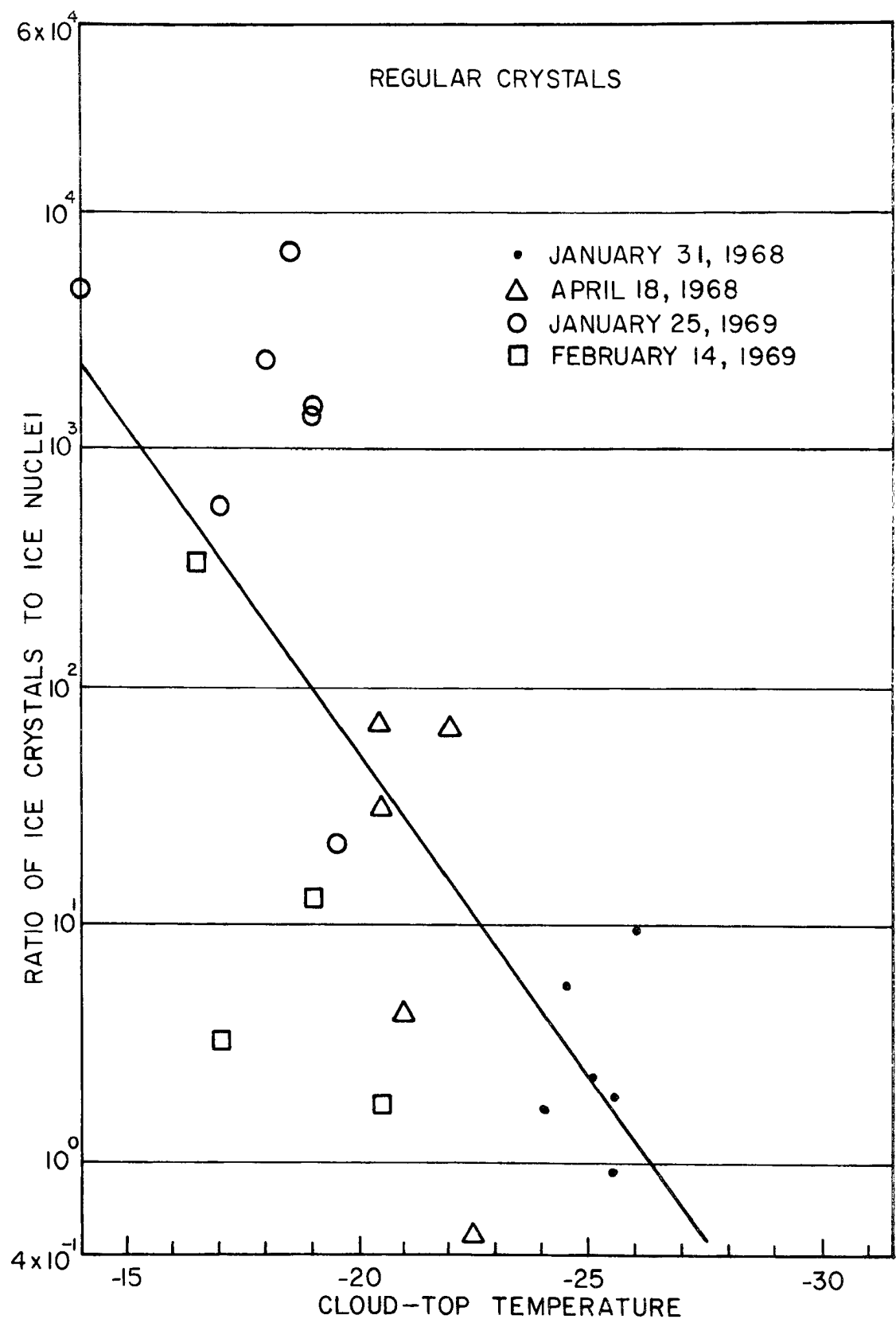


Fig. 13 Ratio of Regular Ice Crystals to Ice Nuclei Versus Cloud-Top Temperature

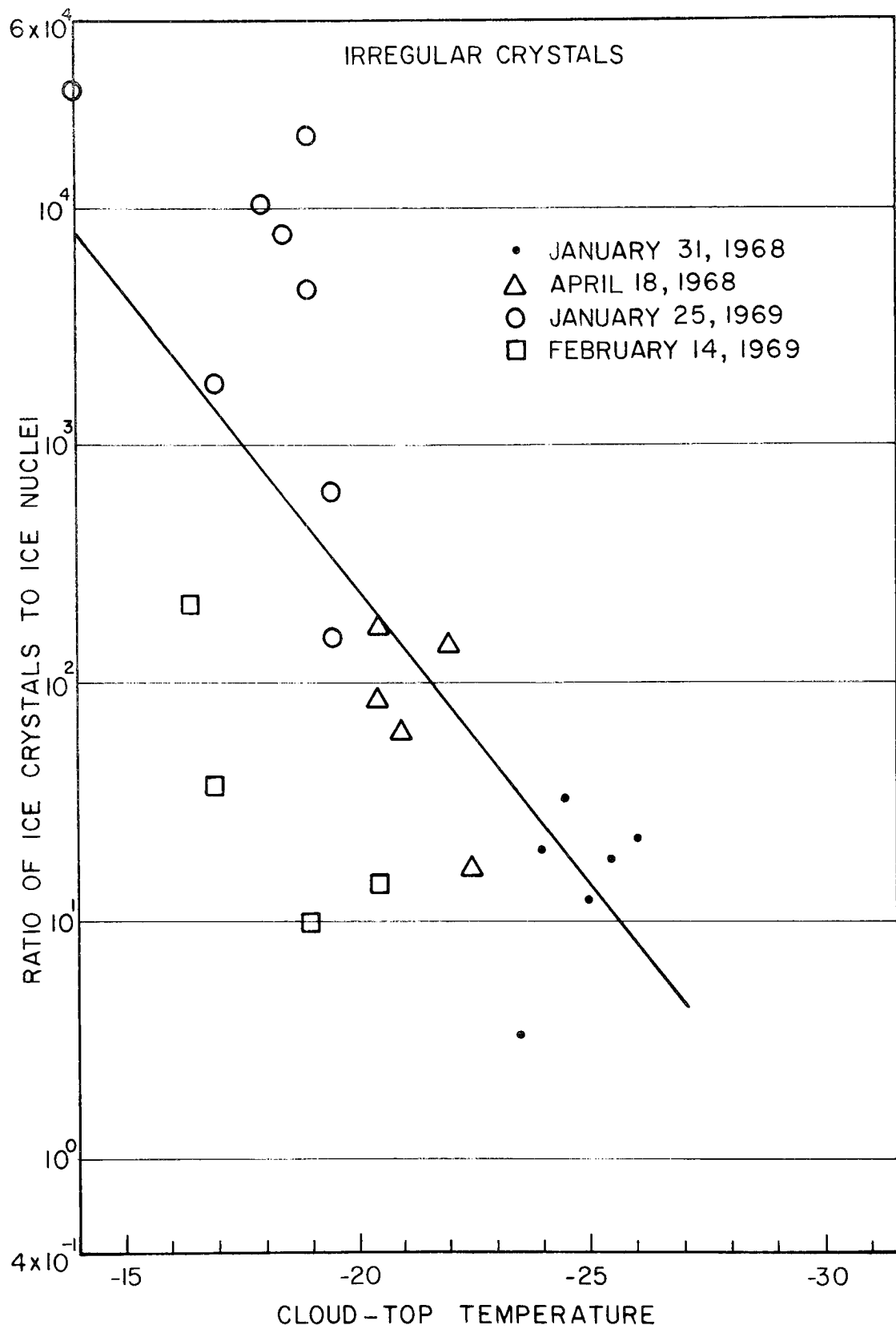


Fig. 14 Ratio of Irregular Ice Crystals to Ice Nuclei Versus Cloud-Top Temperature

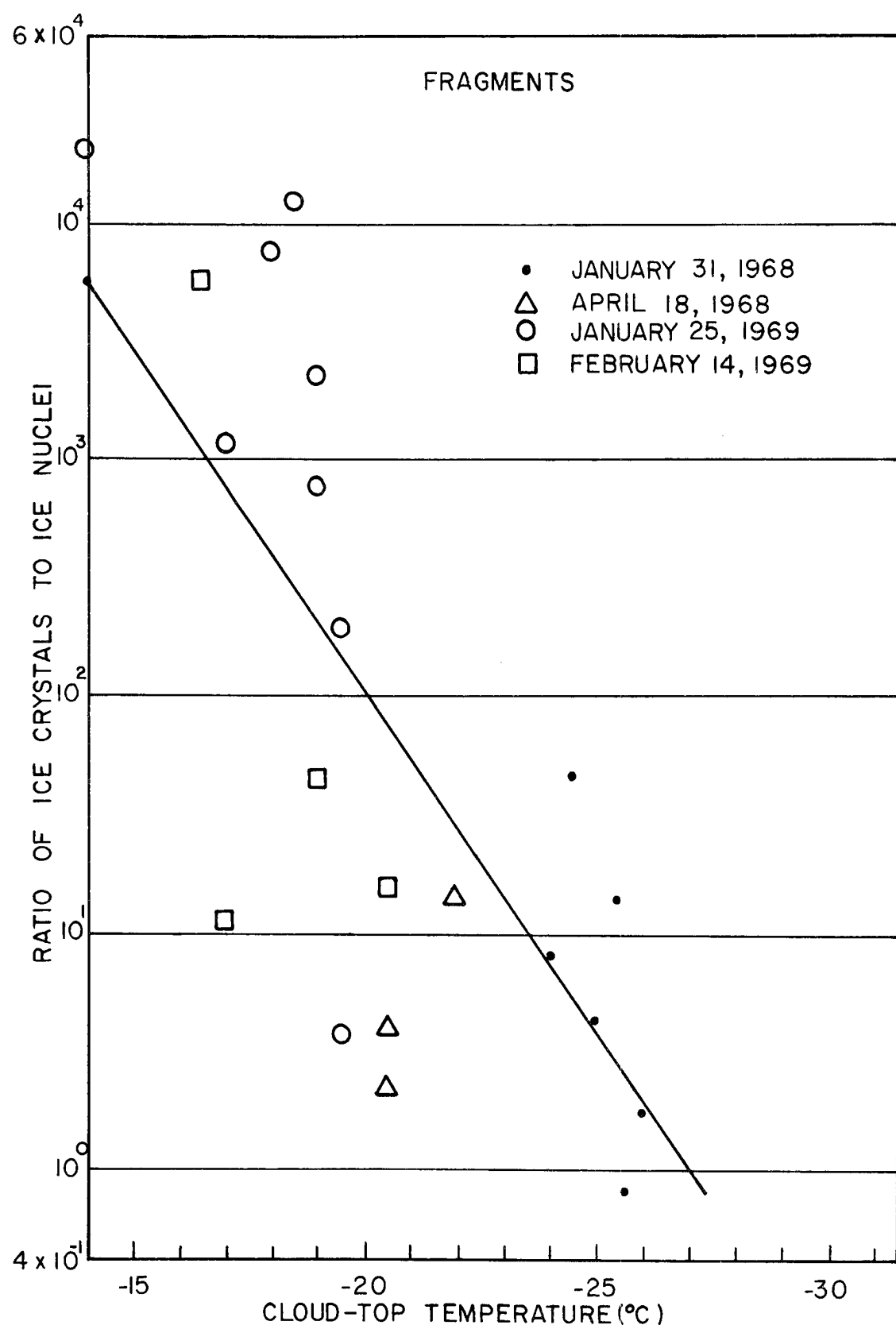


Fig. 15 Ratio of Ice-Crystal Fragments to Ice Nuclei Versus Cloud-Top Temperature

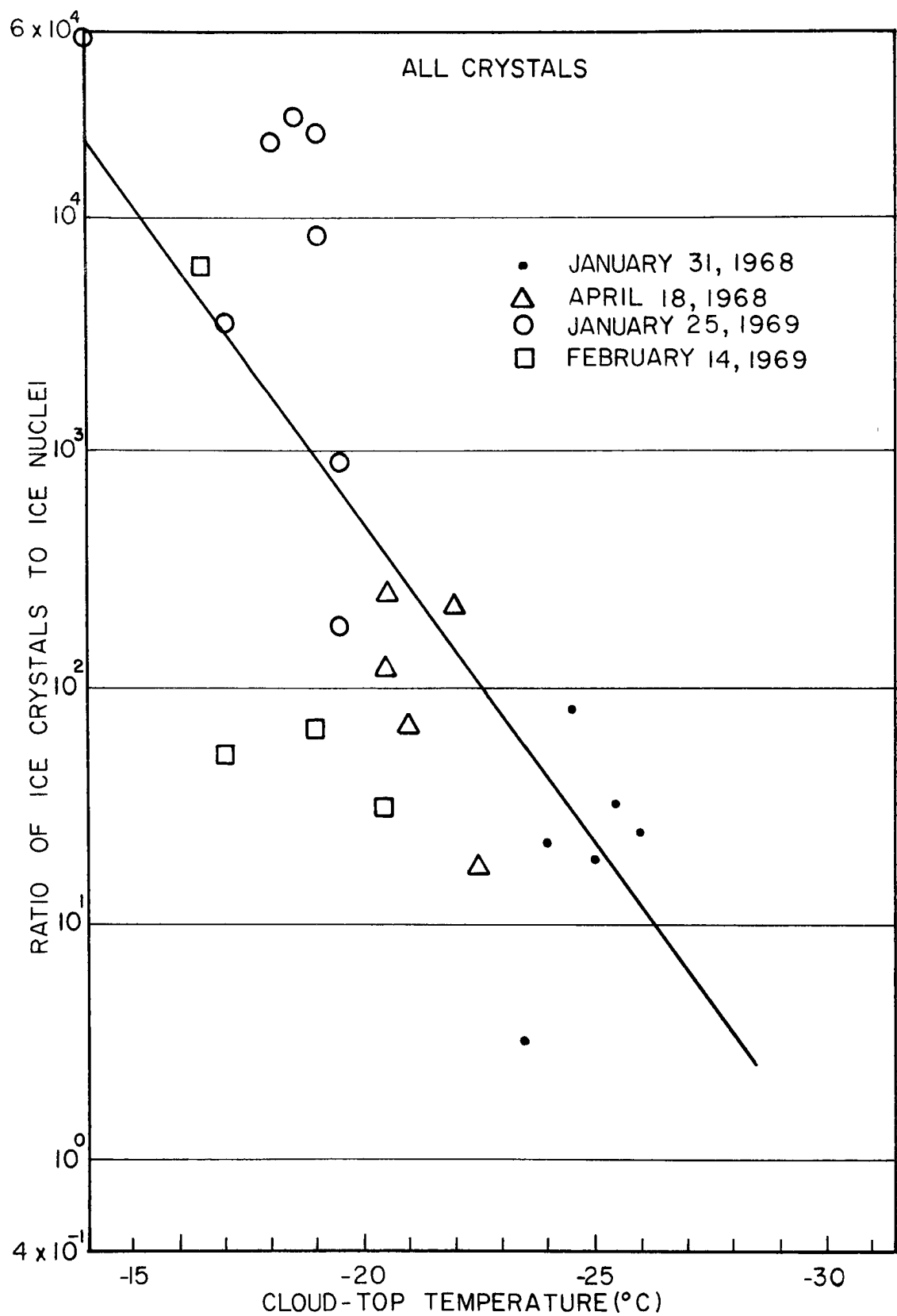


Fig. 16 Ratio of Total Ice Crystals to Ice Nuclei Versus Cloud-Top Temperature

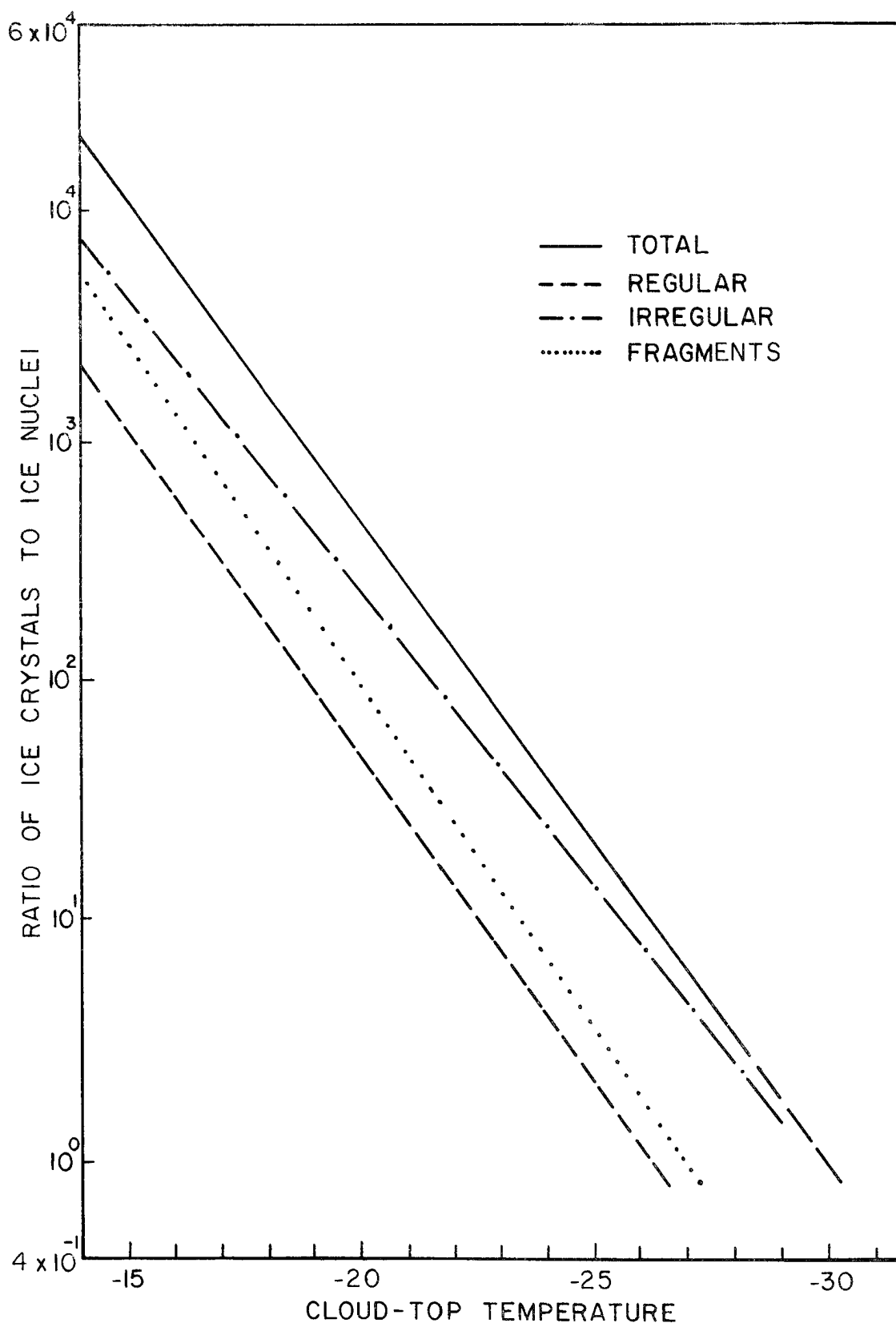


Fig. 17 Composite Plot of Ice-Crystal to Ice-Nuclei Ratios Versus Cloud-Top Temperature

Fig. 3. However, the trend is essentially what one would expect on the cold side of the dendritic region if the multiplication process is due to mechanical fracturing.

Extrapolation of the line for total crystals at the cold end indicates that the ice crystal-ice nuclei ratio becomes one for cloud-top temperatures of -30°C or colder. At the warm end, the ice crystal-ice nuclei ratio becomes greater than 10^4 .

Correlation coefficients for the straight-line regression curves are .69 for Figs. 13, 14, and 15, and .73 for Fig. 16.

DISCUSSION OF RESULTS

Error Analysis

An estimate of the error in the ratio of crystals to ice nuclei is difficult to make because of the extreme range in errors possible. Table 3 gives the more important factors which are measured to calculate the ratio. Probably the most significant factor which was not included in Table 2 is the additional crystal fragments which are blown from trees and other ground sources into the replicator. This effect was shown to be negligible for the storm on February 14, 1969, under low wind-speed conditions but it may not be small under other conditions.

Table 2 includes the extreme errors in various factors on the ratio. The normal method would be to calculate the effect of one standard deviation in the error of a factor on the ratio, but so little information is known about the distribution of errors in some of the factors that it was thought to be more meaningful to consider the extreme ranges.

The collection error due to wind speed is simply the change in density of ice crystals on a flat surface due to the horizontal wind speed. During calm conditions the error is zero, and at greater wind speeds the crystal concentration is underestimated. At a wind speed of five miles per hour the underestimate is approximately a factor of five. This factor is one of several which have an unsymmetrical error distribution. In this case, the error ranges from zero during calm wind conditions, to five times too low at wind speeds of five miles per hour. No ice-crystal concentration data were collected when the winds were greater than five miles per hour.

ELEMENT MEASURED		EXTREME ERROR IN MEASURED ELEMENT	MINIMUM ERROR IN RATIO	MAXIMUM ERROR IN RATIO
ICE CRYSTALS	COLLECTION ERROR DUE TO WIND	+5 KTS	1/5	1
	FALL VELOCITY ERROR DUE TO INCORRECT CLASSIFICATION		1/2	2
	AVERAGING ERROR FOR PEAK CONCENTRATIONS		1/2	1
ICE NUCLEI	BIGG-WARNER MEASUREMENT ERROR		1/5	5
	CLOUD-TOP ESTIMATE ERROR	-2000 FT OR +5°C	1	10
	ERROR IN TEMPERATURE SOUNDING	+ -3°C	1/5	5
TOTAL EXTREME ERROR IN RATIO			1/500	500

Table 3 Extreme Errors in Ice Crystal-Ice Nuclei Ratios

The fall-velocity equations are quite suitable for whole regular crystals, but fragments, irregulars, and rimed crystals are not satisfactorily modeled by these equations. It is felt however, that the fall velocities calculated from these equations are not in error by more than a factor of two either way.

The peaks in ice-crystal concentration were averaged over a fifteen-minute period to better represent a cloud-size crystal population. In some regions of the cloud, a shorter averaging period may be more appropriate. Averaging always reduces the crystal concentrations, thereby making this error factor unsymmetric like the collection factor. The extreme range of the error due to averaging is estimated at a factor of two.

The Bigg-Warner chamber was shown to be in excellent agreement with the standard for ice nuclei adopted at the Second International Workshop on Condensation and Ice Nuclei (1971). However, the adopted standard may not be synonymous with the spectra which clouds activate. The uncertainty in measurements from a Bigg-Warner chamber have been estimated over a wide range depending upon the investigator but, for this paper, the extreme error will be considered as a factor of five high or low.

The cloud tops observed by radar are undoubtedly low which causes the cloud-top temperature to be high. The extreme error is estimated to be low by two thousand feet which corresponds to an error in the ice-nuclei concentration by a factor of ten. Like the collection and averaging errors, the cloud-top estimate is unsymmetrical.

The extreme error in the temperature sounding is estimated to be $\pm 3^{\circ}\text{C}$. This corresponds to a factor of five in the calculation of the ice crystal-ice nuclei ratio.

If the errors were not randomly distributed but were affecting the ratio in the same direction, the minimum and maximum factors of the actual ratio to the calculated ratio would be 1/500 and 500. Even this large error is not sufficient to overcome the high ratio of ice crystals to ice nuclei at warm cloud-top temperatures. In most cases the errors would be more randomly distributed so that the total effect of all the errors is much less. The trend in the ratio of ice crystals to ice nuclei in Fig. 17 is not affected by these error considerations although the extent of ice-crystal multiplication is highly dependent upon them.

Scatter in the Data

Figures 13, 14, 15, and 16 exhibit considerable scatter in the data although the correlation coefficients are near .70. The scatter is evident from storm to storm and even between cells within a storm. It is primarily due to two effects - (1) the error in measurements required to calculate the ratio of ice crystals to ice nuclei and (2) the effect of factors other than cloud-top temperature on ice-crystal multiplication.

Mossop (1967, 1968) pointed out that only a few clouds seem to have the extremely high ratios. The current study seems to bear out this observation. Neglecting the errors which were discussed in the last section, there may be some effect of turbulence due to high wind speeds and wind shears on the ratio. This is reasonable in light of the manner in which mechanical fracturing of ice crystals is thought to

occur. The greater the relative velocities between ice crystals, as in turbulent conditions, the greater the frequency of high-energy collisions which cause fracturing.

To estimate the effect of wind speed on the ice crystal-ice nuclei ratio, the residual from the cloud-top temperature regression was plotted versus the 500-mb. wind for each cell. Figure 18 shows the plot of this residual. There is an obvious trend toward higher ratios at greater wind speeds. If turbulent motions in the cloud can be related to the 500-mb. wind speed, this trend supports the mechanism of mechanical fracturing.

Ice-Crystal-Multiplication Hypothesis

An hypothesis which has not been proved in this thesis, but only strengthened, is the assertion that the ice-crystal multiplication observed is due to mechanical fracturing of fragile dendritic crystals within convective cells. Figure 3 shows the expected shape of the ratio of ice crystals to ice nuclei versus cloud-top temperature, if mechanical fracturing is the cause of increased ice crystals over ice nuclei. Fig. 17 shows a very similar curve for actual data. The proof that mechanical fracturing is the primary mechanism is lacking because no convective clouds with tops warmer than the dendritic region were available from the Climax data. However, many features in the data, such as the presence of crystal fragments in large quantities during passage of convective cells, go a long way toward demonstrating that fragmentation takes place - even though proof is not presently available to show what accounts for the total discrepancy between ice-crystal and ice-nuclei concentrations.

Hindman (1967) averaged the ratio of ice crystals to ice nuclei over several winter orographic storms at Climax and found that the ratio remained less than ten. If the correction factor he used to

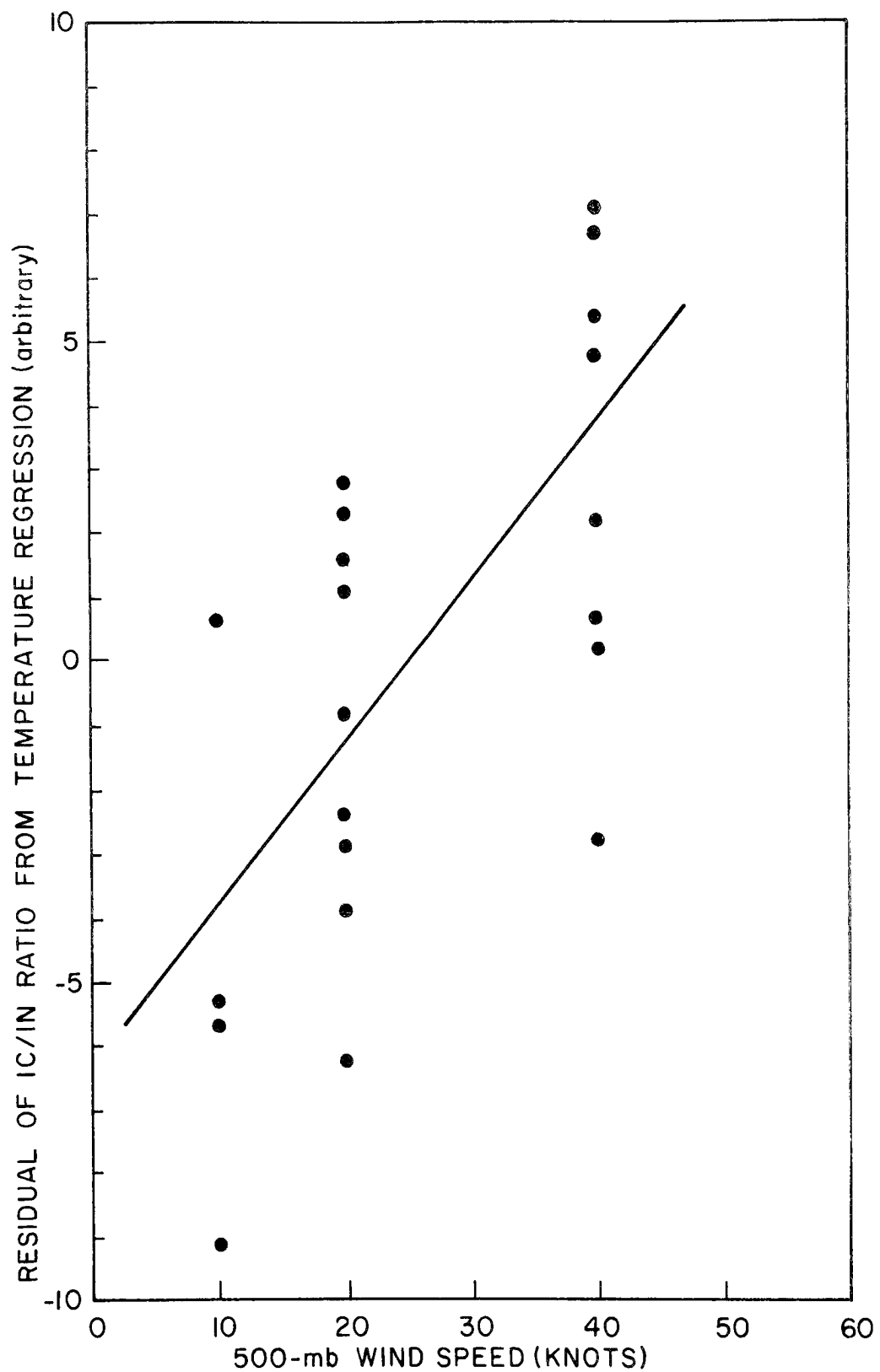


Fig. 18 Residual of IC/IN Ratio from the Temperature Regression Shown in Fig. 16 for Total Crystals Versus the 500-mb Wind Speed

modify the ice-nuclei counts is removed and the irregular crystals are added, the ratio would probably reach 50 or greater for average conditions in his winter orographic storms. In addition, the storms he studied had cloud-top temperatures in the range of -23°C for which the expected ratio for the cells, according to Fig. 17, would be about 100. The two findings are not inconsistent when the frequency of convective cells at the warm temperatures is considered. Convective cells occurring at Climax with cloud-top temperatures near -15°C are quite rare so that the occurrence of clouds with extremely high ice crystal-ice nuclei ratios is low. Also, convective activity does not appear to exist throughout the entire life of an orographic cloud. Some orographic clouds may not contain convective cells at all while others seem to have them throughout their entire lifetime. On the average, orographic clouds appear to contain convective cells during about one-half of the period of their existence. Even with the presence of clouds which have high ice-crystal to ice-nuclei ratios the average ratio could still remain fairly low - on the order of the ratio measured by Hindman.

Since convective cells normally reach colder temperatures than the top of the non-convective orographic cloud, they will nucleate greater concentrations of ice nuclei to seed the lower clouds. Figure 17 indicates that ice-crystal multiplication is contributing to the generation of ice crystals in these cells in addition to this effect. The convective cells then, are efficient mechanisms for providing additional ice crystals to lower orographic clouds which do not contain enough ice crystals to utilize all of the available moisture at certain temperatures. Figure 19 is a photograph of a convective cell in the top of an orographic cloud observed on March 30, 1972. Wind shear

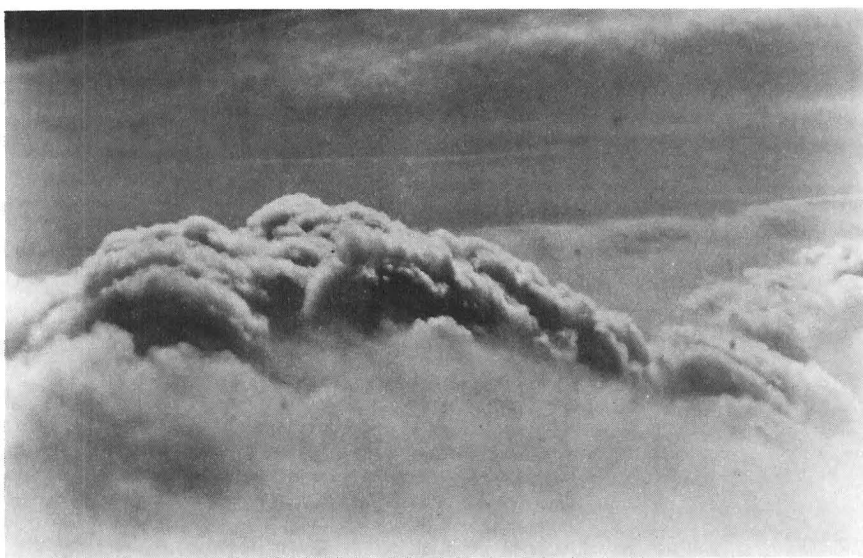


Fig. 19 Example of a Convective Element Embedded in the General Orographic Cloud on March 30, 1972

present at the top of the cloud layer appeared to be producing streamers of ice crystals downwind from similar cells.

Seeding of lower orographic clouds by convective cells agrees with the interesting phenomenon observed by Chappell (1970) that artificial seeding of orographic clouds primarily increases the duration, rather than the intensity, of the precipitation events. Since convective cells are present during only a portion of a storm, the orographic cloud will be seeded naturally and precipitate efficiently only during a fraction of its existence. If, however, the storm is seeded artificially; it will start to precipitate sooner, continue to precipitate longer, and produce greater quantities of precipitation.

Crystal concentrations vary markedly when a storm changes from non-convective to convective conditions. If convective cells are seeding the general orographic cloud, this would explain these abrupt changes. In Fig. D15, a plot of total crystal concentration with time is shown for January 26, 1969. From midnight until seven-thirty, the cloud was convective with a series of convective cells moving through the cloud, but from seven-thirty until noon, it was non-convective. As convective activity increased, the background ice-crystal concentration in and between cells increased. As the convective activity decreased, the opposite occurred. This further strengthens the suggestion that the convective cells are seeding the orographic cloud in which they are embedded.

The hypothesis that ice-crystal multiplication is produced by mechanical fracturing of fragile dendritic crystals within convective cells, and not in the more general orographic cloud, can be tested by comparing ice crystal-ice nuclei ratios in convective and non-convective

orographic clouds. This was not attempted for this thesis because of the difficulty in obtaining cloud-top data by radar for non-convective orographic clouds. This investigation will be attempted at a later date.

Another observation which supports the hypothesis of ice-crystal multiplication in convective cells is the apparent variability in the results of efforts to seed cumulus clouds to increase precipitation by many investigators. If convective clouds are efficient in generating their own ice crystals through ice-crystal multiplication, seeding would not increase the precipitation efficiency, once the ice process is started, and may actually decrease precipitation.

This study then, has presented evidence that ice-crystal multiplication is occurring in convective cells embedded in winter orographic storms, and that mechanical fracturing of fragile dendritic crystals appears to explain the trend in the ice crystal-ice nuclei ratio with temperature. Future studies will extend the statistical study to warmer cloud-top temperatures and will add a more physical approach by studying the shapes and sizes of actual ice crystals which fall from the convective cells.

Impact on Weather Modification

The effects of an ice-crystal-generating mechanism in natural convective clouds can be a very important factor in the production of precipitation and the potential for modification. The computation of seeding potential for orographic clouds must include this effect if it is to approach reality. The seeding potential will depend upon the

extent of ice-crystal multiplication when convective elements are present and the portion of time when the orographic cloud is free of convective elements.

SUMMARY AND RECOMMENDATIONS

Ice-crystal and ice-nuclei concentrations in convective elements of winter orographic storms were compared as a function of cloud-top temperature. The ratio of ice crystals to ice nuclei was found to be greater by a factor of 10^4 at cloud-top temperatures in the dendritic crystal region than at cloud-top temperatures near -30°C . The distribution of the ratios was found to agree with a theoretical distribution which assumes that mechanical fracturing of fragile dendritic crystals is the primary cause of enhanced ice-crystal concentrations. Additional evidence that mechanical fracturing is producing ice-crystal multiplication in convective elements, was the presence of ice-crystal fragments in the peaks of ice-crystal concentrations during cell passages.

Two additional studies should be conducted to verify the hypothesis that ice-crystal multiplication is caused by mechanical fracturing. These are (1) the extension of the present study to warmer cloud-top temperatures to determine if the ratio of ice crystals to ice nuclei becomes less near -10°C where the dendritic region is absent and (2) the determination of the ice crystal-ice nuclei ratio in non-convective orographic clouds to determine if, in fact, convective elements embedded in the orographic clouds are the only source of ice crystals which naturally seed the general cloud layer. A further study, which should indicate if mechanical fracturing is the primary cause, would be a comparison of ice crystal distributions in clouds which are expected to contain fracturing and those which should not contain fracturing.

If the hypothesized mechanism is true, extensive re-examination of the efficiency of natural convective clouds is warranted. Artificial

seeding potential of clouds which contain convective elements will depend upon the initiation, duration, and extent of ice-crystal multiplication due to this mechanism.

REFERENCES

- Auer, A.H., Jr., D.L. Veal, and J.D. Marwitz, 1969: Observations of Ice Crystal and Ice Nuclei Concentrations in Stable Cap Clouds. *J Atmos. Sci.* 26, 1342-1343.
- Auer, A.H. and D.L. Veal, 1970: The Dimensions of Ice Crystals in Natural Clouds. *J. Atmos. Sci.* 27, 919-926.
- Braham, R.R., 1964: What is the Role of Ice in Summer Rain Showers? *J. Atmos. Sci.* 21, 640.
- Brown, S.R., 1970: Terminal Velocities of Ice Crystals. *Atmos. Sci. Paper No. 170*, Colorado State University, Fort Collins, Colorado.
- Chappell, C.F., 1970: Modification of Cold Orographic Clouds. *Atmos. Sci. Paper No. 173*, Colorado State University, Fort Collins, Colorado.
- Fletcher, N.H., 1962: The Physics of Rain Clouds. Cambridge University Press.
- Furman, R.W., 1967: Radar Characteristics of Wintertime Storms in the Colorado Rockies. *Atmos. Sci. Paper No. 112*, Colorado State University, Fort Collins, Colorado.
- Grant, L.O. 1971: The Second International Workshop on Condensation and Ice Nuclei Report. Department of Atmospheric Science, Colorado State University, Fort Collins, Colorado.
- Hallett, J. and B.J. Mason, 1958: The Influence of Temperature and Supersaturation on the Habit of Ice Crystals Grown from the Vapor. *Proc. R. Soc. A* 247, 440, 258-61.
- Hindman, E.E., II, 1967: Snow Crystal and Ice Nuclei Concentrations in Orographic Snowfall. *Atmos. Sci. Paper No. 109*, Colorado State University, Fort Collins, Colorado.
- Hobbs, P.V., 1969: Ice Multiplication in Clouds. *J. Atmos. Sci.*, 26, 315-318.
- Jayaweera, K.O.L.F. and R.E. Cottis, 1969: Fall Velocities of Plate-like and Columnar Ice Crystals. *Quart. J. Roy. Met. Soc.* 95, 703-709.
- Koenig, L.R., 1963: The Glaciating Behavior of Small Cumulonimbus Clouds. *J. Atmos. Sci.*, 20, 29-47.
- _____, 1968: Some Observations Suggesting Ice Multiplication in the Atmosphere. *J. Atmos. Sci.*, 25, 460-463.

- Magono, C. and C.W. Lee, 1966: Meteorological Classification of Natural Snow Crystals. J. Faculty Sci., Hokkaido Univ., Series VII, Vol. 2, No. 4.
- Mason, B.J., 1955: The Physics of Natural Precipitation Processes. Arch. Met. Geophys. Bioklim. A8, 159,207.
- Mossop, S.C., A. Ono, and K.J. Heffernan, 1967: Studies of Ice Crystals in Natural Clouds. J. Rech. Atmos., 3, 45-64.
- Mossop, S.C., 1968: Comparisons Between Concentration of Ice Crystals in Cloud and the Concentration of Ice Nuclei. J. Rech. Atmos., 3, 119-124.
- Nakaya, U., 1954: Snow Crystals, Natural and Artificial. Howard University Press.

APPENDIX A

Ice-Crystal Classification

The replicator films were analyzed by measuring and counting ice crystals according to a modified Magono-and-Lee classification. The crystals were classified into ninety-eight different types, shown in Figs. A1 and A2. Each crystal was assigned a four-digit number to permit calculations to be made on a computer. The first digit indicates the amount of riming. If it is "0", there is no riming but if it is a digit from one to nine, the crystal is rimed 10%, 20%, ..., 90%. If the second digit is a "6", the crystal is a fragment of an identifiable type of crystal. A special type of fragment is the "Sectorlike Fragment". These crystals were classified separately because of the relatively large quantity which were found and because they could not be classified as a fragment of a particular type of crystal. A number of different crystal types have sectorlike extensions and any of them could contribute fragments to this classification. The irregulars include only two classifications but normally make up the majority of ice crystals found at HAO. "Ice Particles" are pieces of ice which have little or no crystalline shape to aid in classification. "Miscellaneous" crystals are pieces of ice which have crystalline shape but do not fit any of the crystal types in Tables A1 and A2.

A computer program, discussed in Appendix B, subdivided the ninety-eight crystal types into eight general categories - Plane Dendrites, Columns, Needles, Plates, Capped Columns, Irregulars, and Sectorlike Fragments. These general categories are useful in handling large quantities of data when one needs to have some information about the

CRYSTAL CLASSIFICATIONS

PLANE DENDRITES

SPATIAL DENDRITES

COLUMNS

	Germ of Skeleton Form			Side Planes			Elementary Sheath			
	X072			X051	X669		X113	X648		
	Stellar Crystal			Scalelike Side Planes			Bundle of Elementary Sheaths			
	X314	X634		X052			X114	X649		
	Ordinary Dendritic Crystal			Combination of Side Planes, Bullets, and Columns			Long Solid Column			
	X315	X635		X053			X115	X650		
	Fernlike Crystal			Plate Aggregate			Combination of Sheaths			
	X316	X636		X054			X122			
	Stellar Crystal with Plates at Ends			Plate with Spatial Plates			Combination of Long, Solid Columns			
	X321	X637		X361	X658		X123			
	Stellar Crystal with Sectorlike Ends			Plate with Spatial Dendrites			Solid Bullet			
	X322	X633		X362	X659		X212	X651		
	Dendritic Crystal with Plates at Ends			Stellar Crystal with Spatial Plates			Hollow Bullet			
	X323	X639		X363	X660		X213	X652		
	Dendritic Crystal with Sectorlike Ends			Stellar Crystal with Spatial Dendrites			Solid Column			
	X324	X640		X364	X661		X214	X653		
	Plate with Dendritic Extensions			Radiating Assemblage of Plates			Hollow Column			
	X327	X643		X371			X215	X654		
	Two-Branched Crystal			Radiating Assemblage of Dendrites			Scroll			
	X331			X372			X218	X657		
	Three-Branched Crystal			Bullet with Dendrites			Combination of Bullets			
	X332			X422	X664		X221			
	Four-Branched Crystal			Stellar Crystal with Needles			Combination of Columns			
	X333			X431	X665		X222			
	Dendritic Crystal with Twelve Branches			Stellar Crystal with Columns						
	X335	X645		X432	X666					
	Stellar Crystal with Scrolls at Ends									
	X433	X667								

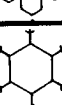
Table A1 Crystal Classifications

CRYSTAL CLASSIFICATIONS

NEEDLES

	Elementary Needle	
	X111	X646
	Bundle of Elementary Needles	
	X112	X647
	Combination of Needles	
	X121	

PLATES

	Pyramid	
	X211	
	Solid Thick Plate	
	X216	X655
	Thick Plate of Skeleton Form	
	X217	X656
	Hexagonal Plate	
	X311	X631
	Crystal with Sectorlike Branches	
	X312	X632
	Crystal with Broad Branches	
	X313	X633
	Plate with Simple Extensions	
	X325	X641
	Plate with Sectorlike Extensions	
	X326	X642
	Broad Branch Crystal with Twelve Branches	
	X334	X644
	Plate with Scrolls at Ends	
	X434	X668

CAPPED COLUMNS

	Column with Plates	
	X411	X662
	Column with Dendrites	
	X412	X663
	Multiple Capped Column	
	X413	
	Bullet with Plates	
	X421	

IRREGULARS

	Ice Particle	
	X061	
	Miscellaneous	
	X064	

SECTORLIKE FRAGMENTS

	Sectorlike Fragment	
		X670

LEGEND

SCHEMATIC OF CRYSTAL	DESCRIPTION OF CRYSTAL	
	CRYSTAL #	FRAGMENT #

Table A2 Crystal Classifications

formation region of the crystals. The formation temperature can be estimated from the general crystal type by considering Table 1 in the theory section.

It is sometimes difficult to identify the dimension of a crystal with which one is working. Table A3 shows the dimensions of the eight general crystal categories and how they were measured. The dimension "D" was perpendicular to the "C" axis of the crystal and the dimension "L" parallel to the "C" axis.

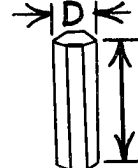
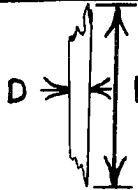
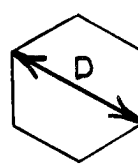
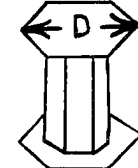
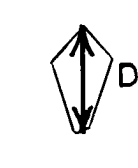
SCHEMATIC	CRYSTAL CLASSIFICATION	COMMENTS
	PLANE DENDRITES	"D" IS THE LONGEST DIMENSION
	SPATIAL DENDRITES	"D" IS THE LONGEST DIMENSION
	COLUMNS	"D" IS THE LONGEST CROSS SECTION
	NEEDLES	"D" IS THE LONGEST CROSS SECTION
	PLATES	"D" IS THE LONGEST CROSS SECTION
	CAPPED COLUMN	"D" IS THE LONGEST CROSS SECTION OF THE "CAP"
	IRREGULARS	"D" IS THE LONGEST DIMENSION
	SECTORLIKE FRAGMENTS	"D" IS THE LONGEST DIMENSION

Table A3 Measurable Crystal Dimensions

APPENDIX B

Fall-Velocity Equations

The fall velocities of ice crystals have been studied by many investigators. Nakaya (1954) is considered to be the standard for ice-crystal fall velocities. However, Nakaya did not have a large data sample, and more refined techniques are now available for measuring fall velocities. In addition, a number of crystal types were not studied by Nakaya.

Brown (1970), using the newer techniques and studying a larger number of crystals, provided more reliable equations with which to calculate fall velocities for ice crystals. Brown did not study columns, fragments, irregular crystals, or rimed crystals, however.

Table B1 shows the fall-velocity equations, adopted primarily from Brown (1970), which were used to calculate crystal concentrations. Plane dendrites, spatial dendrites, needles, plates, capped columns, and the fragments of each, were modeled directly after Brown (1970). Although the fragments are not modeled correctly, this is the best assumption possible at this stage. Columns and their fragments were modeled after a study by Jayaweera and Cottis (1969) and irregular crystals, because of their unpredictable shapes and normally high fall velocities, were modeled with the same equation used for capped columns.

Rimed crystals were modeled by assuming that the fall velocity was simply the unrimed fall velocity multiplied by a "rime factor" depending on the type of crystal and percentage of riming. This concept is valid at Climax because very little riming occurs, and when it does occur,

FALL VELOCITY EQUATIONS

CRYSTAL CLASSIFICATION	FALL VELOCITY EQUATION
PLANE DENDRITES FRAGMENTS OF PLANE DENDRITES	$8.4D^{0.217}$
SPATIAL DENDRITES FRAGMENTS OF SPATIAL DENDRITES	$3.71D^{0.38}$
COLUMNS FRAGMENTS OF COLUMNS	$-10.863 + .5707D + 3.088 \times 10^{-4}L$ $-8.954 \times 10^{-4}D^2 + 4.371 \times 10^{-6}LD$ $-1.215 \times 10^{-8}L^2$
NEEDLES FRAGMENTS OF NEEDLES	$2.17L^{0.455}$
PLATES FRAGMENTS OF PLATES SECTORLIKE FRAGMENTS	$1.10D^{0.525}$
CAPPED COLUMNS FRAGMENTS OF CAPPED COLUMNS IRREGULARS	$0.92L^{0.65}$
RIMED PLANE DENDRITES RIMED FRAGMENTS OF PLANE DENDRITES	$8.4D^{0.217} [1 + (13.3P / 5.6D^{0.377})]$
RIMED SPATIAL DENDRITES RIMED FRAGMENTS OF SPATIAL DENDRITES	$3.71D^{0.38} [1 + (13.3P / 2D)]$
RIMED COLUMNS RIMED FRAGMENTS OF COLUMNS	$[-10.863 + .5707D + 3.088 \times 10^{-4}L$ $-8.954 \times 10^{-4}D^2 + 4.371 \times 10^{-6}LD$ $-1.215 \times 10^{-8}L^2] \times [1 + (13.3P / 2D)]$
RIMED NEEDLES RIMED FRAGMENTS OF NEEDLES	$2.17L^{0.455} [1 + (13.3P / 2D)]$
RIMED PLATES RIMED FRAGMENTS OF PLATES RIMED SECTORLIKE FRAGMENTS	$1.10D^{0.525} [1 + (13.3P / 4.04D^{0.449})]$
RIMED CAPPED COLUMNS RIMED FRAGMENTS OF CAPPED COLUMNS RIMED IRREGULARS	$0.92L^{0.65} [1 + (13.3P / 2D)]$

Table B1 Fall-Velocity Equations

the crystals are normally covered by a single layer of rimed droplets.

The theoretical derivation of the "rime factor" follows.

The assumption is made that the terminal velocity of an unrimed crystal is proportional to the square root of the volume, which is valid for a high percentage of the small plate-like crystals at Climax. Therefore,

$$v(\text{unrimed}) = kV^{\frac{1}{2}} = k(At)^{\frac{1}{2}} = k't^{\frac{1}{2}} \quad (1)$$

where k = constant

k' = new constant

V = volume of crystal

A = area of crystal normal to fall direction

t = thickness of crystal normal to fall direction

The fall velocity of a rimed crystal is greater by some incremental amount than that of an unrimed crystal of the same size.

$$v(\text{rimed}) = v(\text{unrimed}) + dv(\text{unrimed}) \quad (2)$$

But,

$$dv(\text{unrimed}) = \frac{1}{2} k't^{-\frac{1}{2}} dt = \frac{1}{2} k't^{\frac{1}{2}} \frac{dt}{t} \quad (3)$$

Substituting (1) into (3) and (3) into (2), the fall velocity of a rimed crystal in terms of an unrimed crystal becomes,

$$v(\text{rimed}) = v(\text{unrimed}) \left[1 + \frac{1}{2} \frac{dt}{t} \right] \quad (4)$$

where dt = the additional thickness of the crystal due to riming in a single layer.

The additional thickness of a crystal due to riming depends upon the number of droplets covering the crystal and their size.

$$\frac{dt}{dt} = \frac{n \cdot V_d}{A} \quad (5)$$

where n = number of droplets rimed on crystal of area A

V_d = volume of rimed droplets

The number of droplets can be estimated by the percent coverage of a crystal and the size of the droplets.

$$n = \frac{P \cdot A}{A_d} \quad (6)$$

where P = percent coverage of the crystal by droplets

A_d = cross-sectional area of a droplet

Substituting (6) into (5),

$$\frac{dt}{dt} = \frac{PV_d}{A_d} = \frac{4}{3} Pr \quad (7)$$

where r = radius of droplets

Assuming that the rimed droplets are 20 microns in diameter, equation (4) becomes,

$$v(\text{rimed}) = v(\text{unrimed}) \left[1 + 6.65 \frac{P}{t} \right] \quad (8)$$

The only remaining unknown variable in equation (8) is the thickness of the crystals, t . Auer and Veal (1970) reported the results of a study they made which predicts the expected thickness of a crystal knowing its diameter or length. Using Auer and Veal's best

fit curves for thickness, the "rime factor" for each crystal type can be obtained. The lower portion of Table B1 shows the appropriate equation for each type of rimed crystal.

Crystal Concentrations

Once the fall velocities are known, the concentration of ice crystals can be determined from the following equation,

$$C = \frac{N \cdot S}{W \cdot v \cdot A'}, \quad (9)$$

where C = concentration of crystals

N = number of crystals observed on film

S = rate of movement of film past slit opening in replicator

W = slit width of replicator

v = fall velocity of ice crystal

A' = area of film inspected

Equation (9) is used to determine individually the concentration of each type and size of crystal observed on the replicator film. These individual concentrations can then be summed into any classification scheme desired. Figure B1 shows one such computation and classification routine. This computer flow chart shows the method by which crystals are sorted by type and size, their concentrations computed, and reclassified into 28 sub-groupings. An additional task of this particular program was the calculation of collision frequencies between crystals, which is not discussed in this thesis. Table B2 shows an example of the output from this computer program. Such a listing of crystal concentrations was made for each five minutes during all of the storms studied. To facilitate the assimilation of the huge

SITE - HAO DATE - 690214

TIME	TYPE	V-VEL	EXPTM	LENGTH	WIDTH	N/LITER	NUMBR	STEMP	TIME	TYPE	V-VEL	EXPTM	LENGTH	WIDTH	N/LITER	NUMBR	STEMP
0125	0636	45.7	24.39	2450.	0.	.199	1	-10	0125	0054	47.3	24.39	810.	0.	.193	1	-10
0125	0054	40.8	24.39	550.	0.	.223	1	-10	0125	0631	20.0	24.39	250.	0.	.456	1	-10
0125	0311	20.0	24.39	250.	0.	.456	1	-10	0125	0312	25.9	24.39	410.	0.	.352	1	-10
0125	0311	17.3	24.39	190.	0.	.527	1	-10	0125	0325	37.0	24.39	810.	0.	.246	1	-10
0125	0642	29.0	24.39	510.	0.	.314	1	-10	0125	0638	34.3	24.39	650.	0.	.266	1	-10
0125	0325	35.5	24.39	750.	0.	.256	1	-10	0125	0311	33.0	24.39	650.	0.	.276	1	-10
0125	0635	38.5	24.39	1110.	0.	.237	1	-10	0125	0637	29.9	24.39	350.	0.	.304	1	-10
0125	1054	39.7	24.39	510.	0.	.229	1	-10	0125	1635	39.7	24.39	1190.	0.	.230	1	-10
0125	0311	25.2	24.39	390.	0.	.361	1	-10	0125	1642	29.6	24.39	510.	0.	.308	1	-10
0125	0311	18.2	24.39	210.	0.	.500	1	-10	0125	1054	36.6	24.39	410.	0.	.249	1	-10
0125	0633	33.0	24.39	650.	0.	.276	1	-10	0125	0313	35.5	24.39	750.	0.	.256	1	-10
0125	0312	34.5	24.39	710.	0.	.264	1	-10	0125	0311	30.2	24.39	550.	0.	.302	1	-10
0125	0311	27.2	24.39	450.	0.	.335	1	-10	0125	0325	30.2	24.39	550.	0.	.302	1	-10
0125	0321	41.4	24.39	1550.	0.	.220	1	-10	0125	0638	40.5	24.39	1410.	0.	.225	1	-10
0125	0311	25.9	24.39	410.	0.	.352	1	-10	0125	0327	41.1	24.39	1510.	0.	.222	1	-10
0125	2635	40.5	24.39	1210.	0.	.225	1	-10	0125	0315	42.9	24.39	1830.	0.	.212	1	-10
0125	0670	13.0	24.39	110.	0.	.37918	54	-10	0125	0670	15.3	24.39	150.	0.	11.933	20	-10
0125	0670	18.2	24.39	210.	0.	.12001	24	-10	0125	0670	20.0	24.39	250.	0.	.2282	5	-10
0125	0670	22.4	24.39	310.	0.	.2853	7	-10	0125	0670	23.8	24.39	350.	0.	.2677	7	-10
0125	0670	25.9	24.39	410.	0.	.3519	10	-10	0125	0670	27.2	24.39	450.	0.	.1005	3	-10
0125	0670	29.0	24.39	510.	0.	.628	2	-10	0125	0061	29.7	24.39	210.	0.	.919	3	-10
0125	0061	33.3	24.39	250.	0.	.821	3	-10	0125	0061	38.3	24.39	310.	0.	1.903	8	-10
0125	0061	45.9	24.39	410.	0.	.595	3	-10	0125	0061	48.8	24.39	450.	0.	.747	4	-10
0125	0061	52.9	24.39	510.	0.	.344	2	-10	0125	0061	59.5	24.39	610.	0.	.306	2	-10
0125	0061	65.6	24.39	710.	0.	.278	2	-10									

***** TABLE OF SUMMED CONCENTRATIONS *****

PDENDRITE	SDENDRITE	COLUMNS	NEEDLES	PLATES	CCOLUMNS	IRREGULAR	TOTAL REGULAR
.654	.416	0.000	0.000	4.786	0.000	.5.914	5.856
FPDENDRITL	FSDENDRITF	FCOLUMN	FNEEDLES	FPLATES	FCCOLUMNS	FSECTIRS	TOTAL FRAGMENTS
1.231	0.C00	0.000	0.000	1.046	0.000	74.416	77.094
RPDENDRITE	RSDENDRITE	RCOLUMN	RNEEDLES	RPLATES	RCCOLUMNS	RREGULARS	TOTAL RIMED REG.
0.000	.479	0.000	0.000	0.000	0.000	0.000	.479
RFPDENDRITE	RFSDENDRITE	RFCOLUMN	RFNEEDLES	RFPLATES	RFCOLUMNS	RFSECTORS	TOTAL RIMED FRAGMENTS
.455	0.000	0.000	0.000	.308	0.000	0.000	.762
TPDENDRITE	TSDFNDRITF	TCOLUMN	TNEEDLES	TPLATES	TCOLUMNS	TIRREGULARS	TOTAL CRYSTALS
2.340	.895	0.000	0.000	6.140	0.000	5.914	84.191
***** THERE WERE 191. TOTAL CRYSTALS *****							
***** ALL CRYSTALS 90.105							

***** SUMS OF COLLISION FREQUENCIES *****

PDEN-PDEN	SDEN-SDEN	COLL-COLL	NEDL-NEDL	PLAT-PLAT	CCOL-CCOL	IRRG-IRRG	SECT-SECT
.617E-03	.181E-04	0.	0.	.924E-03	0.	.954E-03	.193E-01
PDEN-SDEN							
.256E-03							
PDEN-COLL	SDEN-CCLL						
0.	0.						
PDEN-NEDL	SDEN-NEDL	COLL-NEDL					
0.	0.	0.					
PDEN-PLAT	SDEN-PLAT	COLL-PLAT	NEDL-PLAT				
.506E-02	.598E-03	0.	0.				
PDEN-CCOL	SDEN-CCUL	COLL-CCOL	NEDL-CCOL	PLAT-CCOL			
0.	0.	0.	0.	0.			
POEN-IRRG	SDEN-IRRG	COLL-IRRG	NEDL-IRRG	PLAT-IRRG	CCOL-IRRG		
.288E-02	.346E-03	0.	0.	.326F-02	0.		
PDEN-SECT	SCFN-SECT	COLL-SECT	NEDL-SECT	PLAT-SECT	CCOL-SECT	IRRG-SECT	TOTAL COLLISIONS NORMALIZED TOTAL
.830E-01	.744E-02	0.	0.	.214F-01	0.	.314F-01	.177 .197E-02

Table B2 Example of Output from Crystal-Classification Program

quantities of data, the output from this program was fed into another computer program which averaged the ice-crystal data over fifteen-minute running means and plotted them automatically. An example of such a plot is shown in Fig. D13.

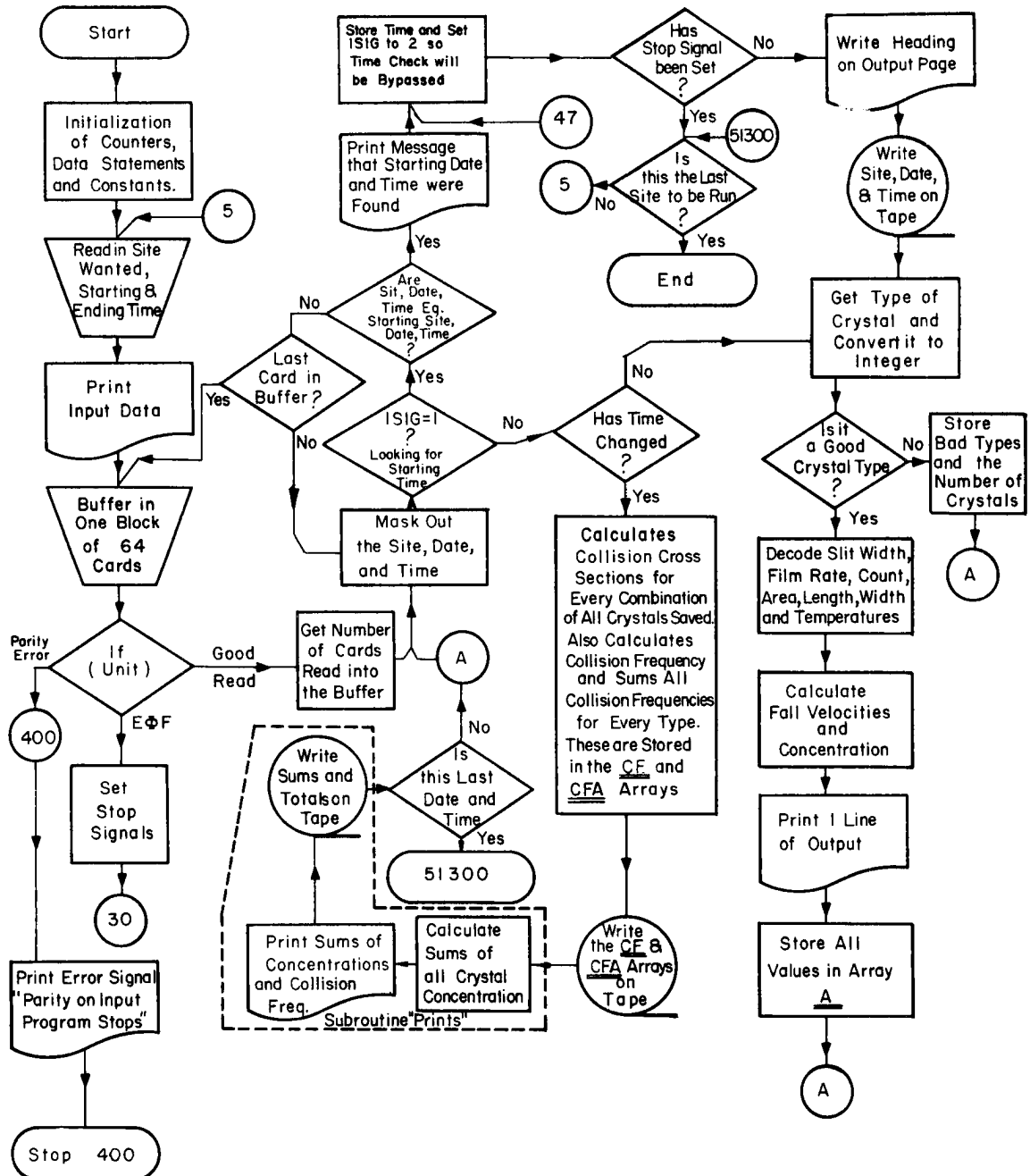


Fig. B1 Computer Program Flow Chart

APPENDIX C

Trajectory Model

A model which predicts the delay time, from the first appearance of a convective cell on the radar until the subsequent fallout of ice crystals into the replicator, is required in order to identify which radar echo produces a given peak in ice-crystal concentration. A trajectory model was developed from the geometry of the cloud movements shown in Fig. C1. Position "A" corresponds to the point at which ice crystals begin to fall relative to the earth. The crystals are then at a distance "d" from, and a height "H" above, the ice-crystal replicator. Position "B" corresponds to the point at which the convective cell first intersects the radar beam and the cloud height determined. The ice-crystal trajectories are shown by the dashed line and are at a height "y" above the surface. Position "C" is the location of the replicator and the radar. Only a slight correction was required in the subsequent calculations when the replicator was positioned at HAO rather than near the radar on Chalk Mountain. The horizontal wind profile, shown as "u", was determined from synoptic observations and radar cloud movements.

The following assumptions were made in the model.

1. There was no change in the cloud from point A to point B.
2. The ice crystals had a constant fall velocity of 30 cm/sec.
3. The horizontal wind-speed profile was linear with height and zero at the surface.

If the time at point "A" is arbitrarily set equal to zero, then the desired delay time is given by:

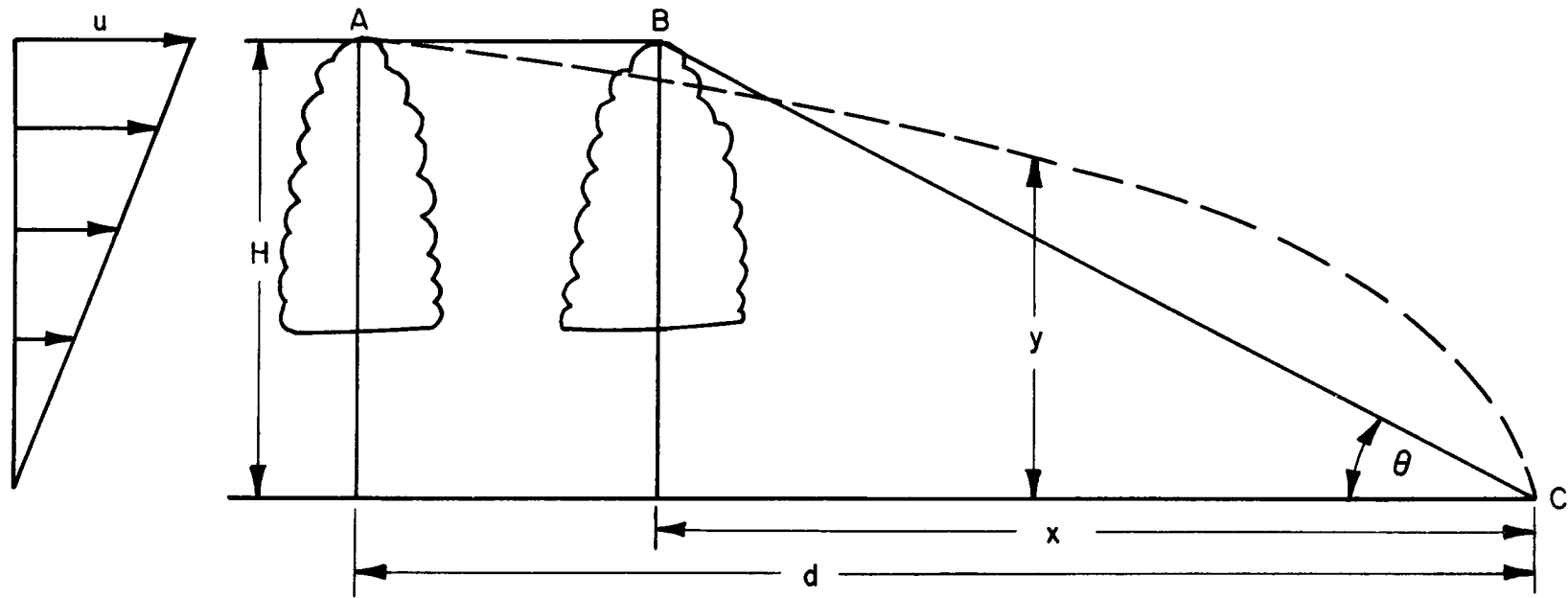


Fig. C1 Geometry of Radar Beam and Ice-Crystal Trajectories

$$T_D = T_f - T_R \quad (1)$$

where

T_D = delay time from the first appearance of a cell on the radar to the entrance of the crystals from the same cell into the replicator.

T_f = total time of fall for the crystals from point "A" to point "C".

T_R = elasped time from point "A" to point "B".

Now, T_f may be written:

$$T_f = \frac{H}{v} \quad (2)$$

where

H = radar height of the cloud equal to $X \tan \theta$, where X is the horizontal range of the cloud at point "B" and θ is the elevation angle of the radar.

v = fall velocity of crystals

Also, T_R may be written:

$$T_R = \frac{d-x}{u_c} \quad (3)$$

where

d = total horizontal distance of crystal trajectory.

x = horizontal range of cloud at point "B".

u_c = horizontal speed of cloud

Now, d is:

$$d = \int_0^{T_f} u dt \quad (4)$$

where

u = horizontal speed of the ice crystals.

But, u may be written:

$$u = ky \quad (5)$$

where

k = a constant determined by observation.

$$y = H - vt \quad (6)$$

Substituting (5) and (6) into (4) and integrating,

$$d = kHT_f - \frac{kv}{2} T_f^2. \quad (7)$$

Substituting (7) into (3) and (2) and (3) into (1)

$$T_D = \frac{H}{v} - \frac{kH^2}{u_c v} + \frac{kH^2}{2vu_c} + \frac{x}{u_c} \quad (8)$$

But

$$u_c = kH \quad (9)$$

and

$$x = \frac{H}{\tan \theta} \quad (10)$$

therefore

$$T_D = \frac{H}{2v} + \frac{1}{k \tan \theta} \quad (11)$$

For a wind profile, where the horizontal wind is 25 knots at 6000 feet above the surface, the delay time as a function of cloud height is shown in Fig. C2. From this plot, it can be seen that the delay time varies from 45 minutes to 2 1/2 hours. However, at low cloud heights, one would expect the delay time to approach zero. This is not true in

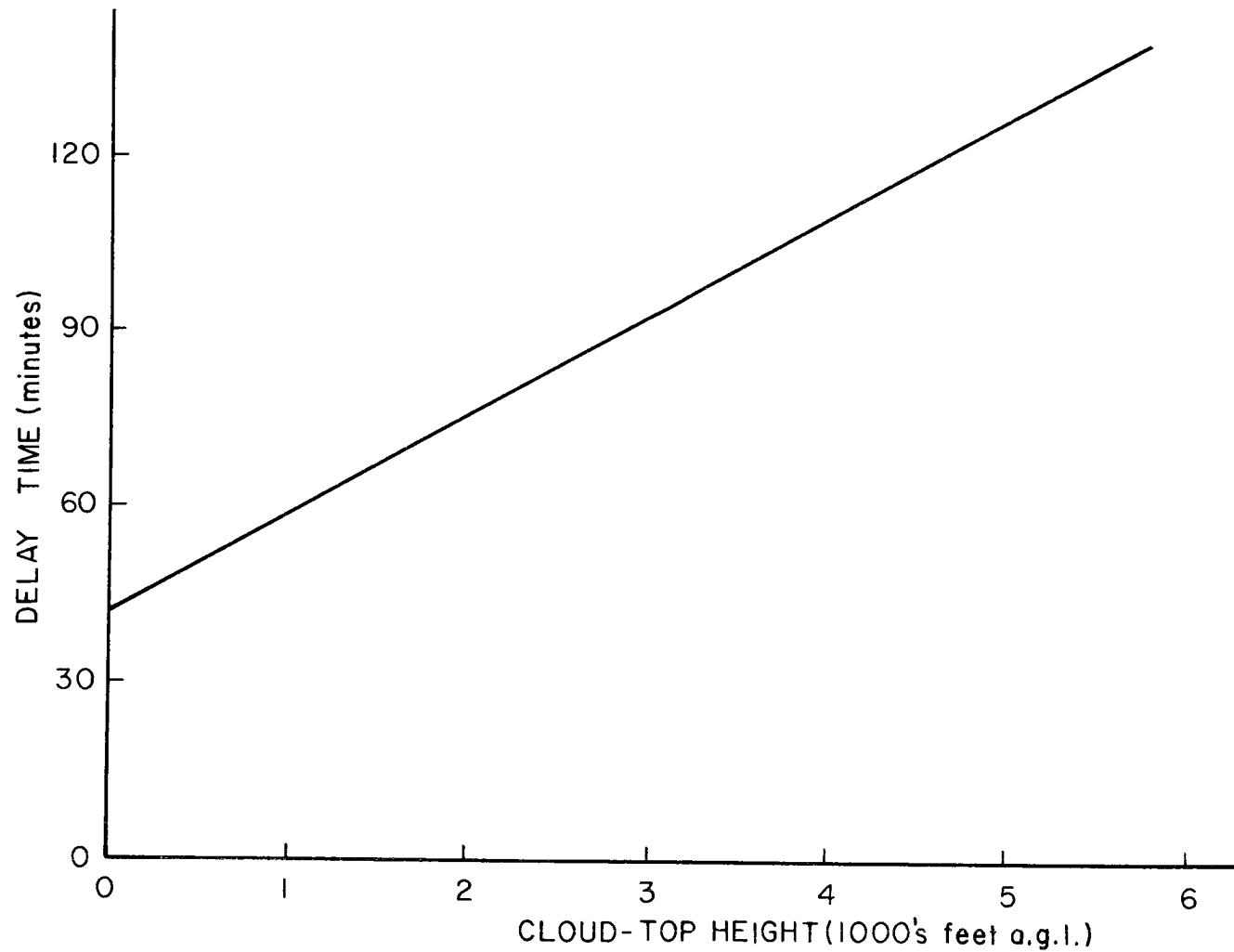


Fig. C2 Ice-Crystal Delay Time from the First Observation of the Cloud on Radar
to the Entrance of Crystals into the Replicator

this formulation because of the assumed wind profile $u = ky$. For other profiles, such as $u = \text{constant}$, the delay time does approach zero as H approaches zero, but are not reasonable in other respects. All of the clouds treated in this study were 3000 feet or more above the radar so the formulation appeared satisfactory. When predicted peaks were compared with actual peaks, the agreement was surprisingly good, considering the assumptions made in the model.

APPENDIX D

Data

Included in this appendix are the basic data which were used in the study. Radar data, except for a table of cloud tops for the cells studied, were not included because of the volume of data studied. The Figures and the Table should be self-explanatory, and a listing of the order in which they are arranged is given in the Table of Contents.

74

CELL NUMBER	CLOUD HEIGHT	CLD.-TOP TEMP.	CONC. NUCLEI	CONC. REG.	CONC. IRREG.	CONC. FRAG.	CONC. TOTAL	RATIO REG.	RATIO IRREG.	RATIO FRAG.	RATIO TOTAL
JANUARY 31, 1968											
1	17750	-23.5	1.95	0	6.32	0	6.32	0	3.24	0.	3.24
2	18080	-24.0	2.20	3.60	44.10	1.77	49.50	1.64	20.0	.81	22.5
3	18420	-26.0	3.90	3.59	86.68	6.84	96.92	1.92	22.2	1.75	24.9
4	17750	-24.5	2.60	14.05	85.23	118.89	214.84	5.40	32.8	45.7	82.6
5	18080	-25.5	3.40	6.16	62.94	47.38	116.48	1.81	18.5	13.9	34.3
6	17750	-25.0	3.00	6.51	36.87	13.30	56.67	2.17	12.3	4.43	18.9
APRIL 18, 1968											
7	18080	-22.0	1.70	112.44	238.86	22.57	373.91	66.1	141.	13.3	220.
8	17070	-20.5	.68	47.04	120.19	2.76	169.99	69.2	177.	4.06	250.
9	17400	-21.0	.92	3.92	59.07	0	63.00	4.26	64.2	0	68.5
10	18080	-22.5	2.30	1.07	38.78	0	39.84	.465	16.9	0	17.3
11	17070	-20.5	.68	21.09	59.16	1.46	81.71	31.0	87.0	2.15	120.
JANUARY 25, 1969											
12	18750	-18.5	.0125	82.10	95.23	156.00	333.33	6568.	7618.	12480.	26670.
13	18420	-18.0	.0095	22.01	97.42	71.73	191.17	2316.	10250.	7550.	20120.
14	18750	-19.0	.0165	24.23	75.46	36.39	136.09	1468.	4573.	2205.	8247.
15	18750	-19.0	.0165	22.66	336.94	12.78	372.37	1373.	20420.	775.	22570.
16	16050	-14.0	.0010	4.68	31.64	20.65	56.97	4680.	31640.	20650.	56970.
17	18750	-19.5	.0220	1.57	14.07	4.32	19.96	71.4	640.	196.	907.
18	18750	-19.5	.0220	.46	3.43	.08	3.98	20.9	156.	3.64	181.
19	17400	-17.0	.0054	3.03	9.99	6.42	19.11	561.	1850.	1188.	3538.
FEBRUARY 14, 1969											
20	15370	-16.5	.0170	5.49	3.58	95.50	104.58	323.	211.	5617.	6151.
21	16380	-19.0	.2000	2.43	1.95	8.89	13.27	12.2	9.75	44.5	66.4
22	17070	-20.5	.3750	.61	5.35	5.83	11.79	1.63	14.3	15.5	31.4
23	15370	-17.0	.0860	.27	3.19	.96	4.42	3.14	37.1	11.2	51.4

Table D1 Summary of Data: Cloud Height in Feet Above Sea Level, Cloud-Top Temperature in Degrees Centigrade, and Ice Nuclei and Ice Crystal Concentrations in Number Per Liter

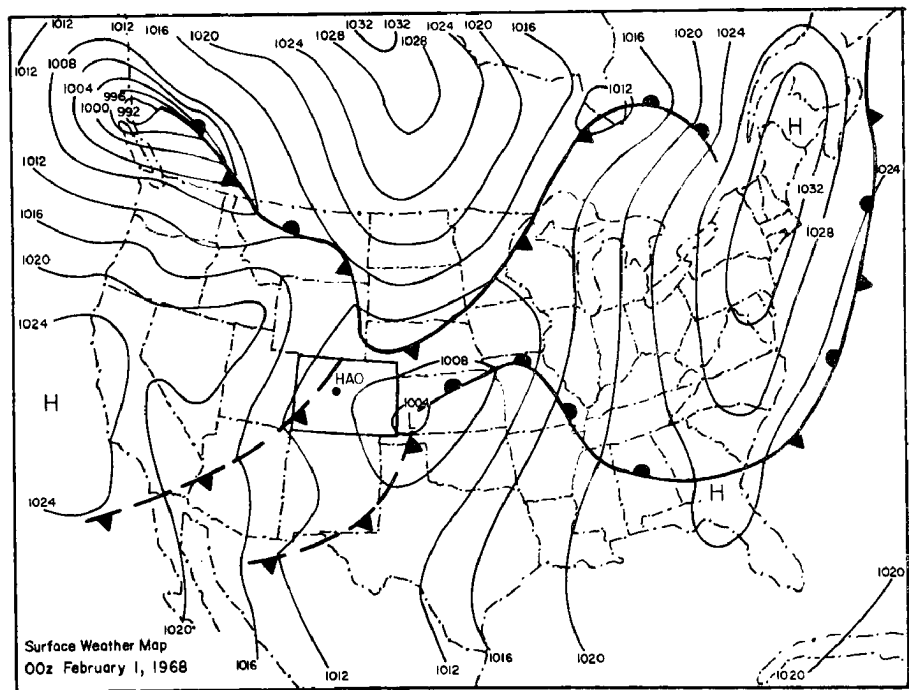
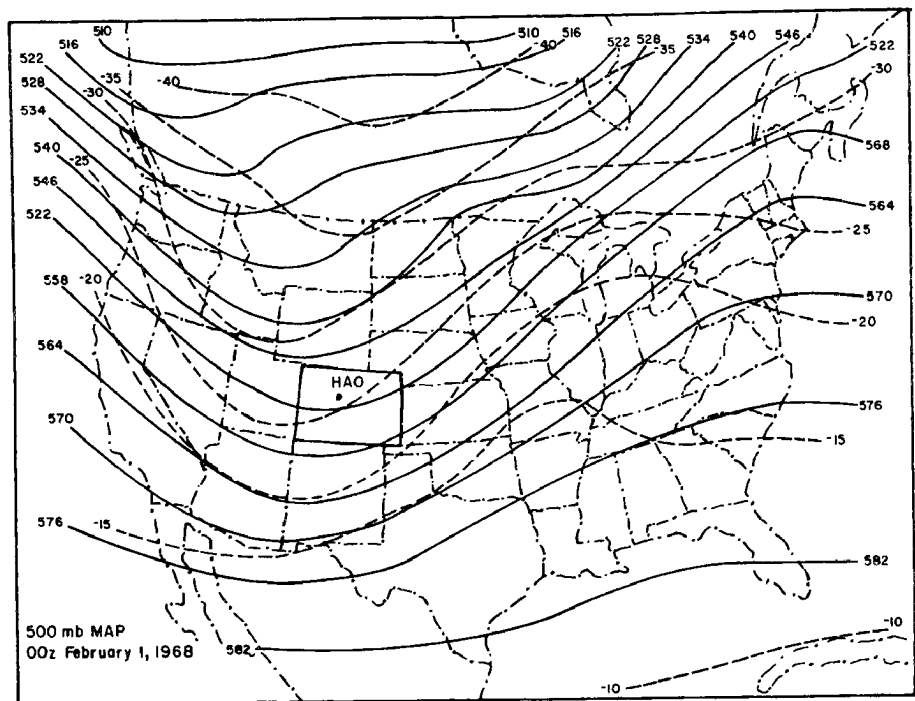


Fig. D1 Synoptic Maps for January 31, 1968

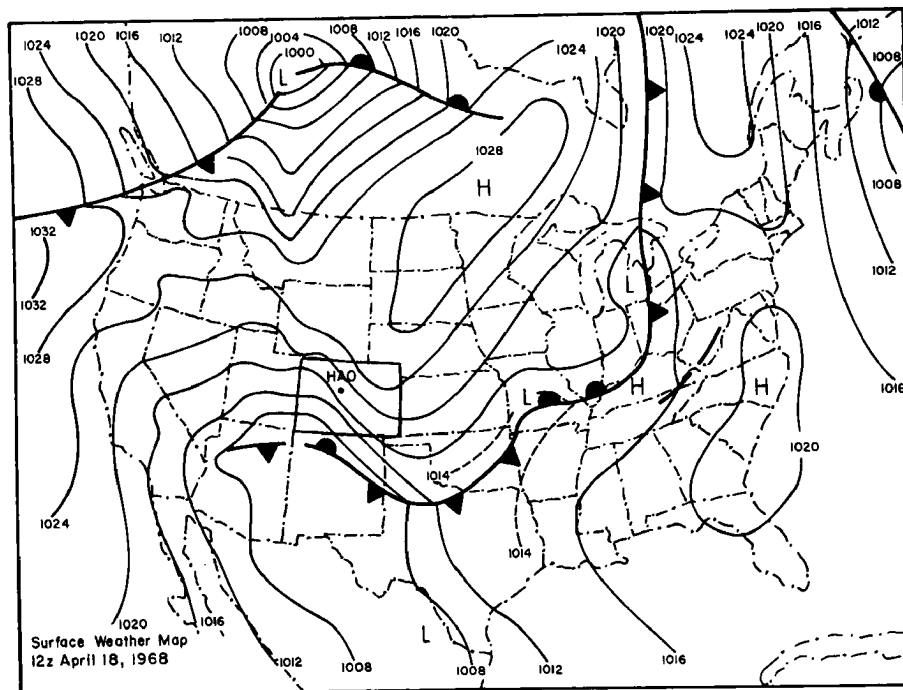
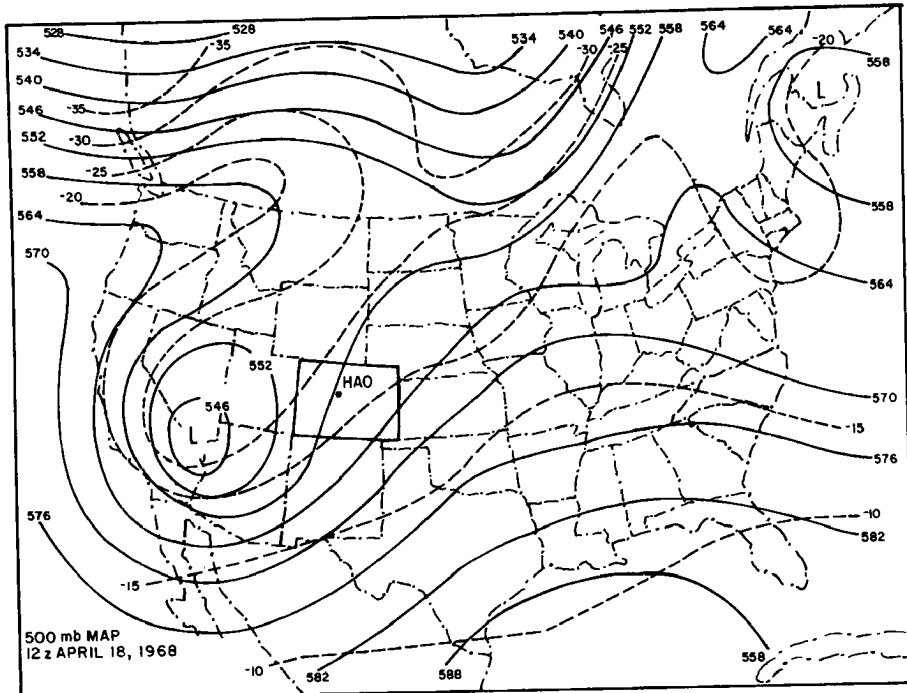


Fig. D2 Synoptic Maps for April 18, 1968

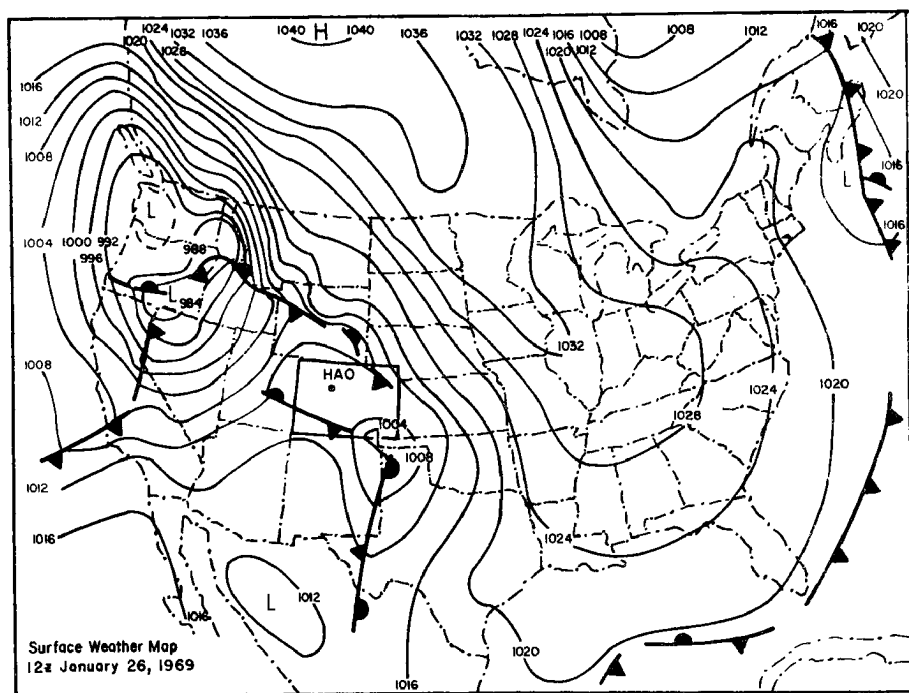
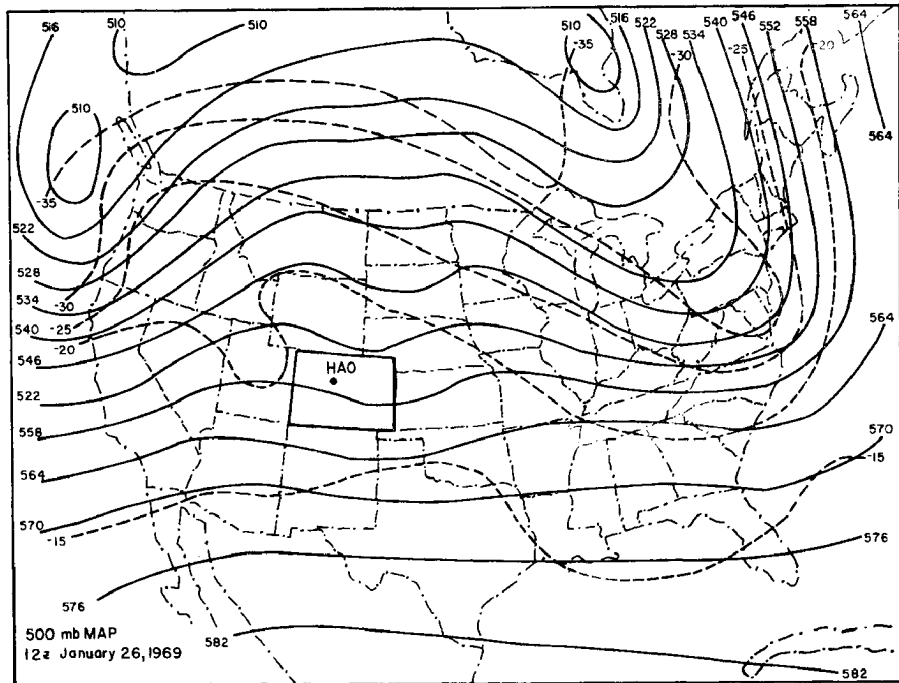


Fig. D3 Synoptic Maps for January 25, 1969

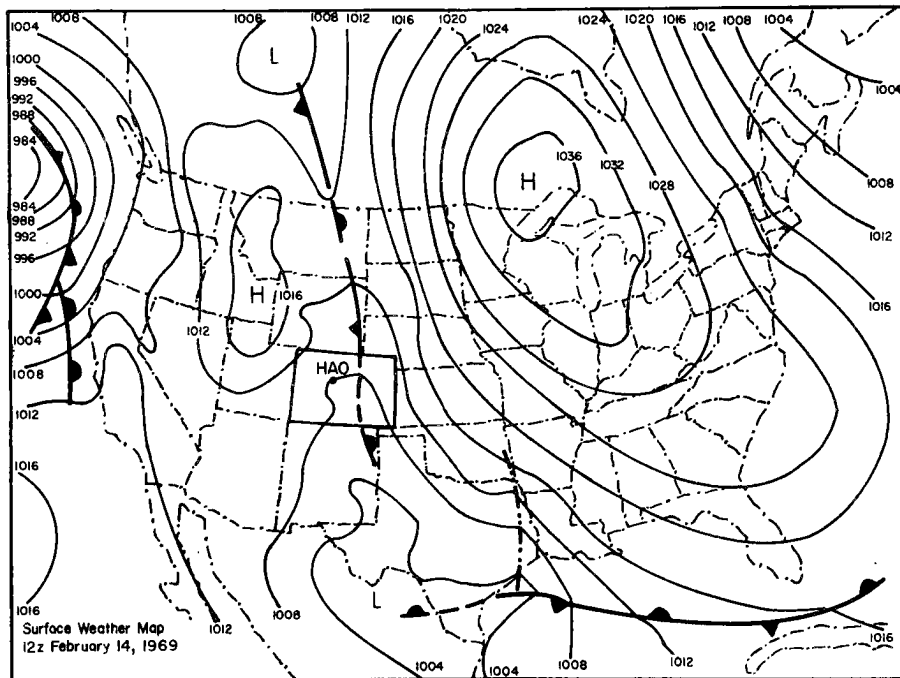
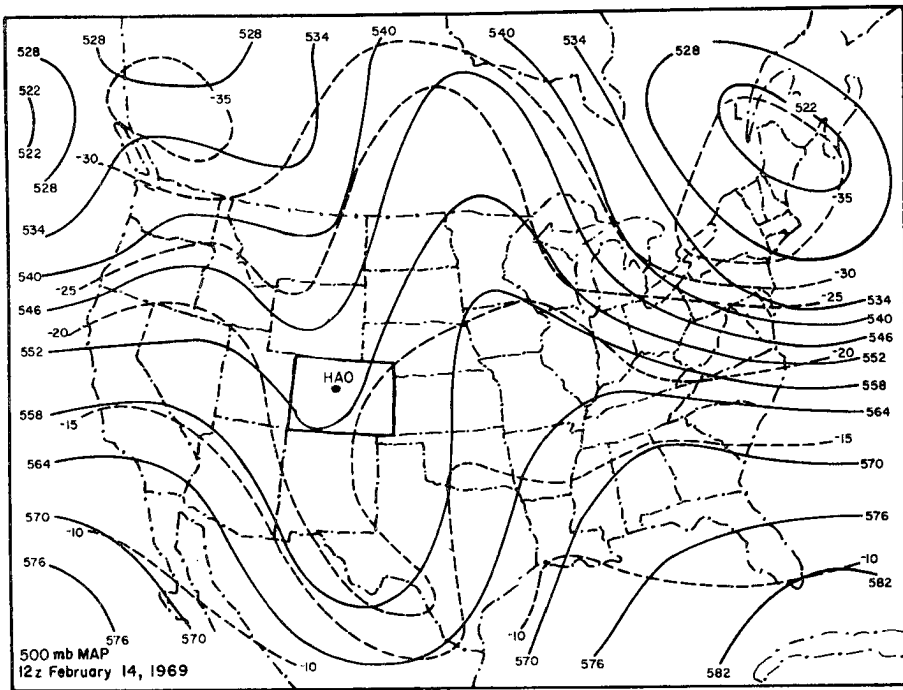


Fig. D4 Synoptic Maps for February 14, 1969

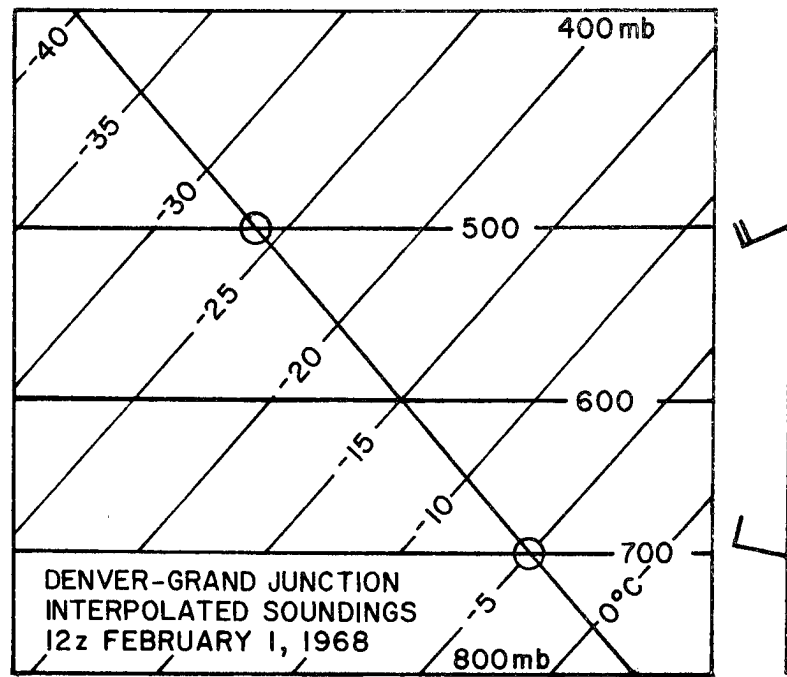


Fig. D5 Temperature Sounding and Winds for Climax
on January 31, 1968

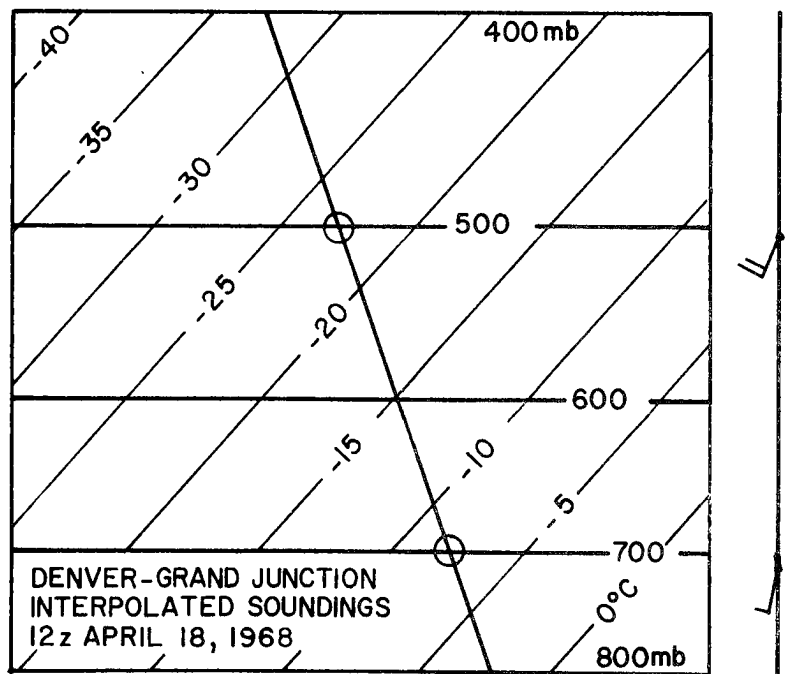


Fig. D6 Temperature Sounding and Winds for Climax
on April 18, 1968

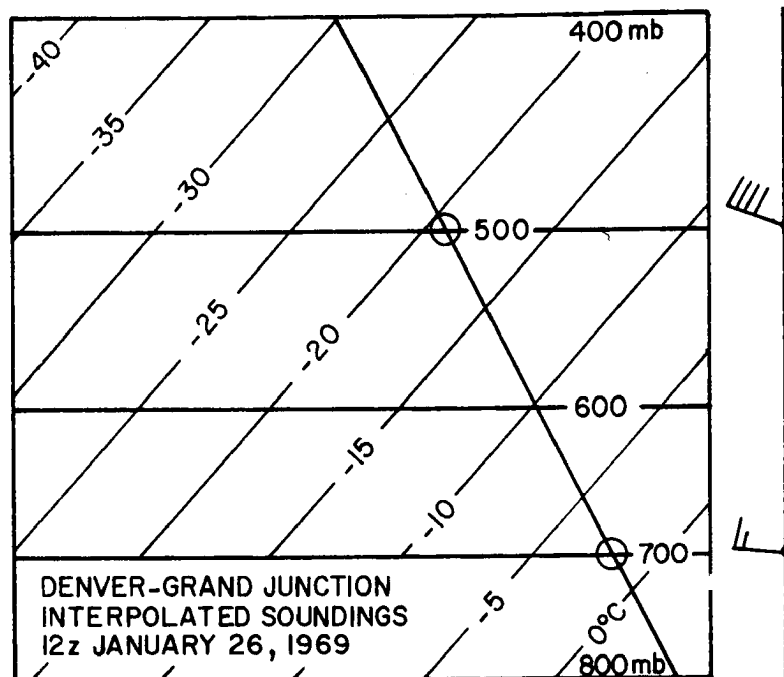


Fig. D7 Temperature Sounding and Winds for Climax
on January 25, 1969

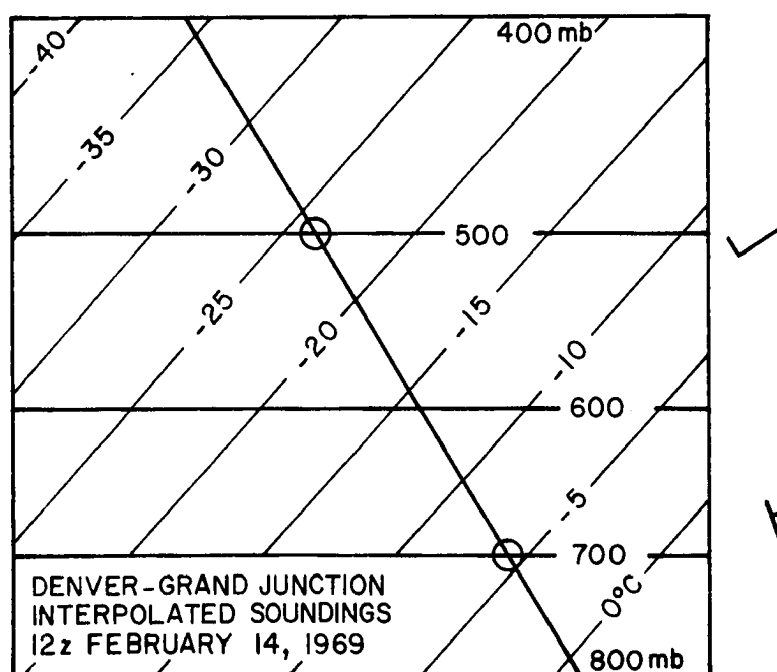


Fig. D8 Temperature Sounding and Winds for Climax
on February 14, 1969

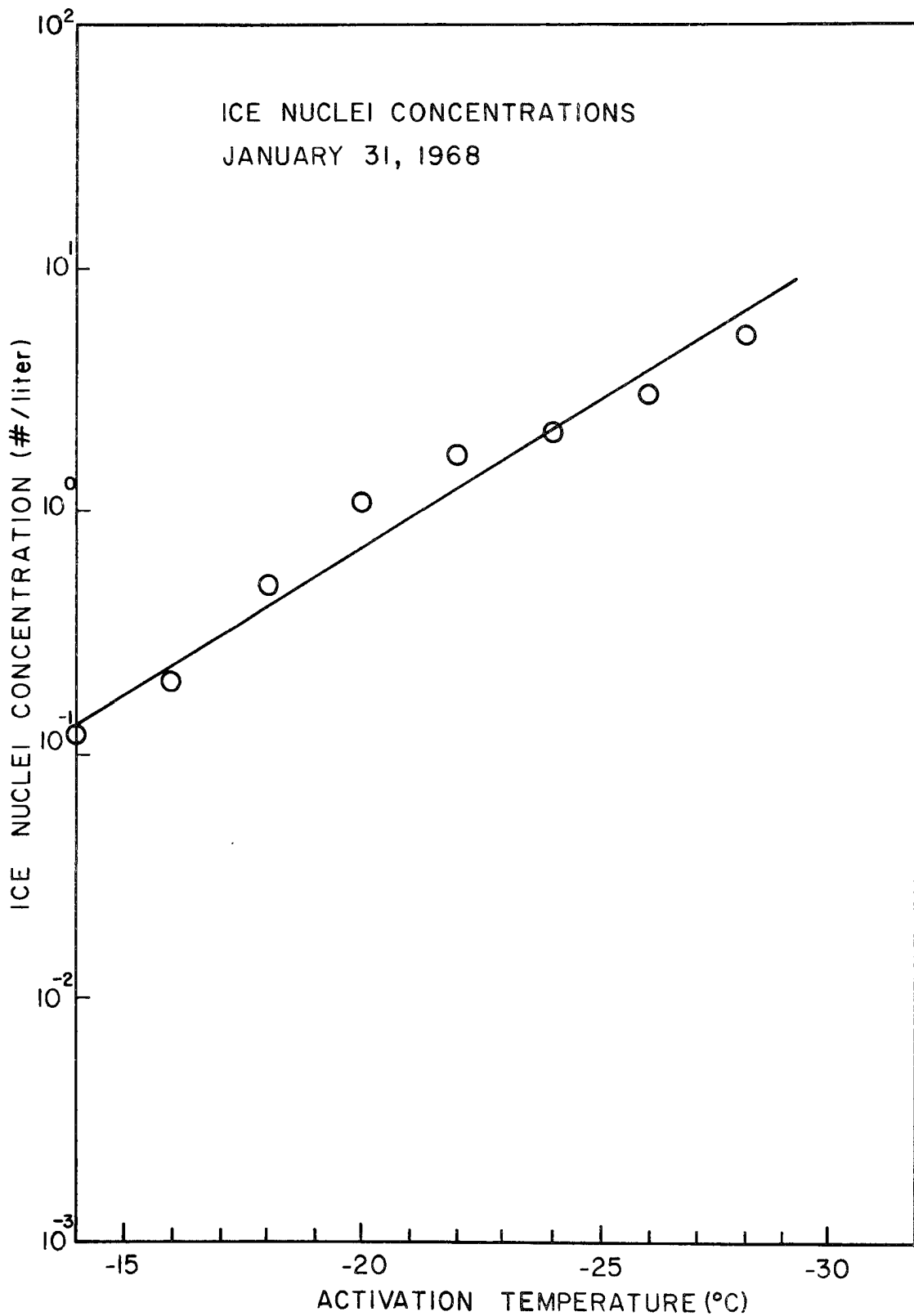


Fig. D9 Ice-Nuclei Spectrum for January 31, 1968

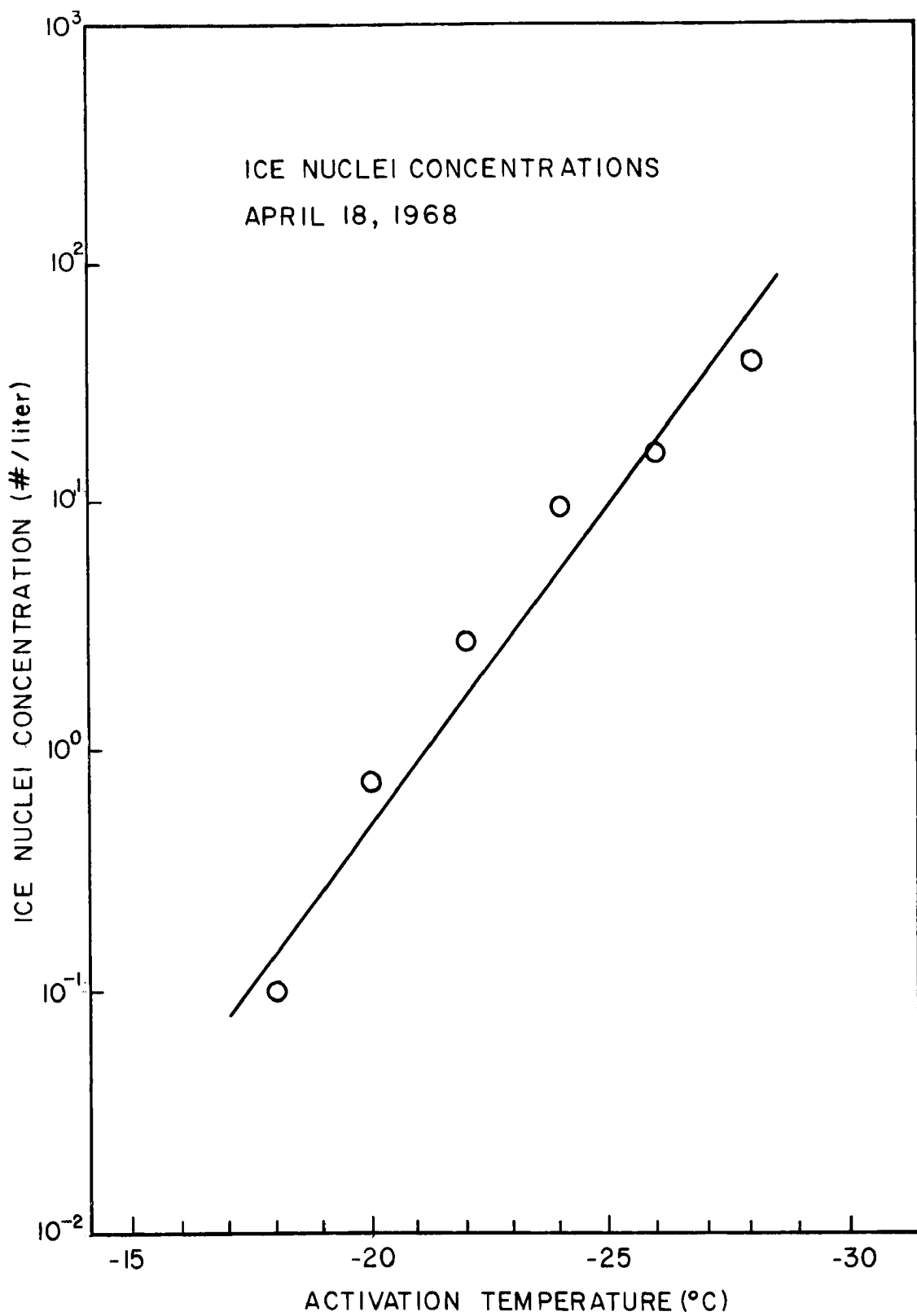


Fig. D10 Ice-Nuclei Spectrum for April 18, 1968

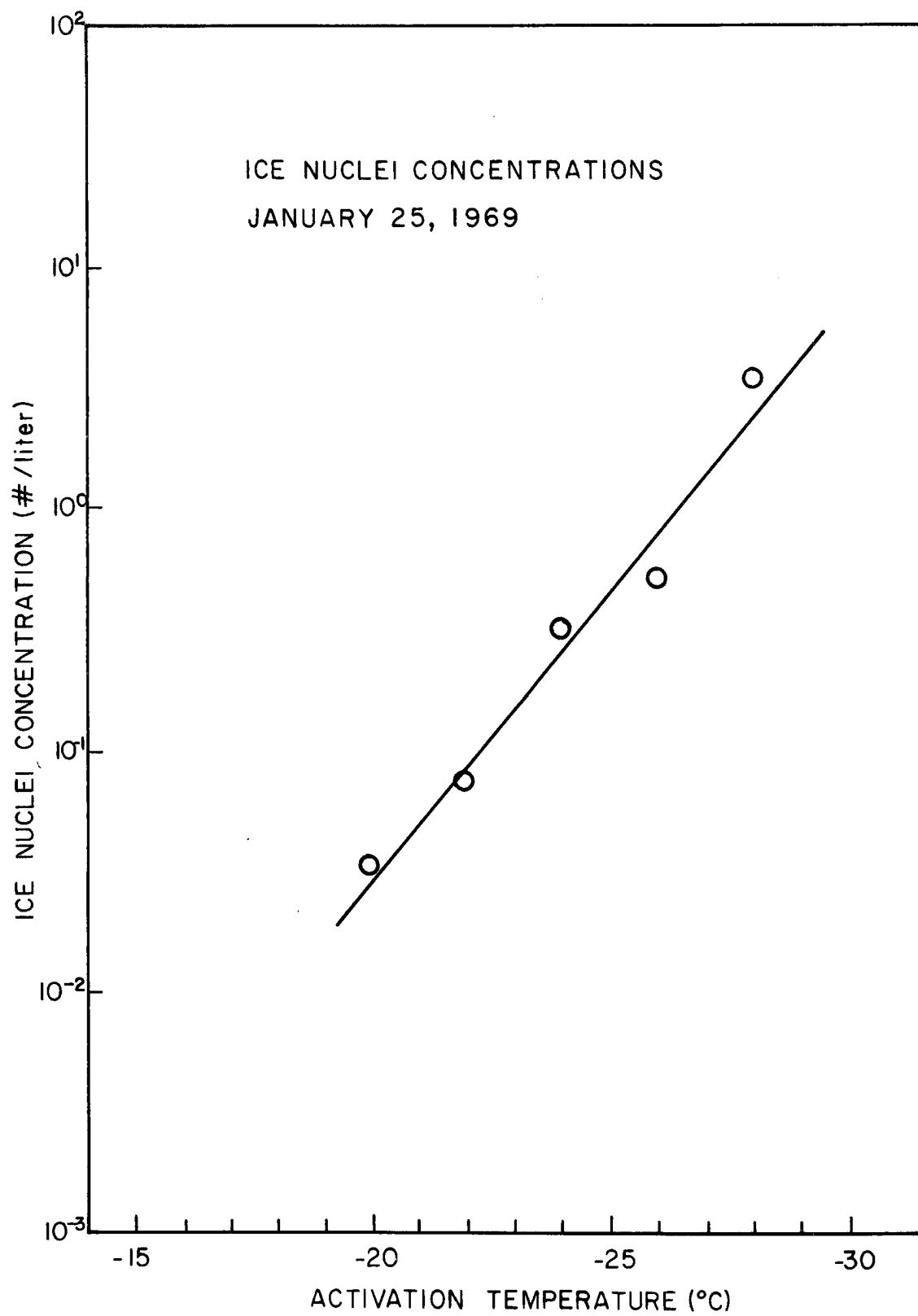


Fig. D11 Ice-Nuclei Spectrum for January 25, 1969

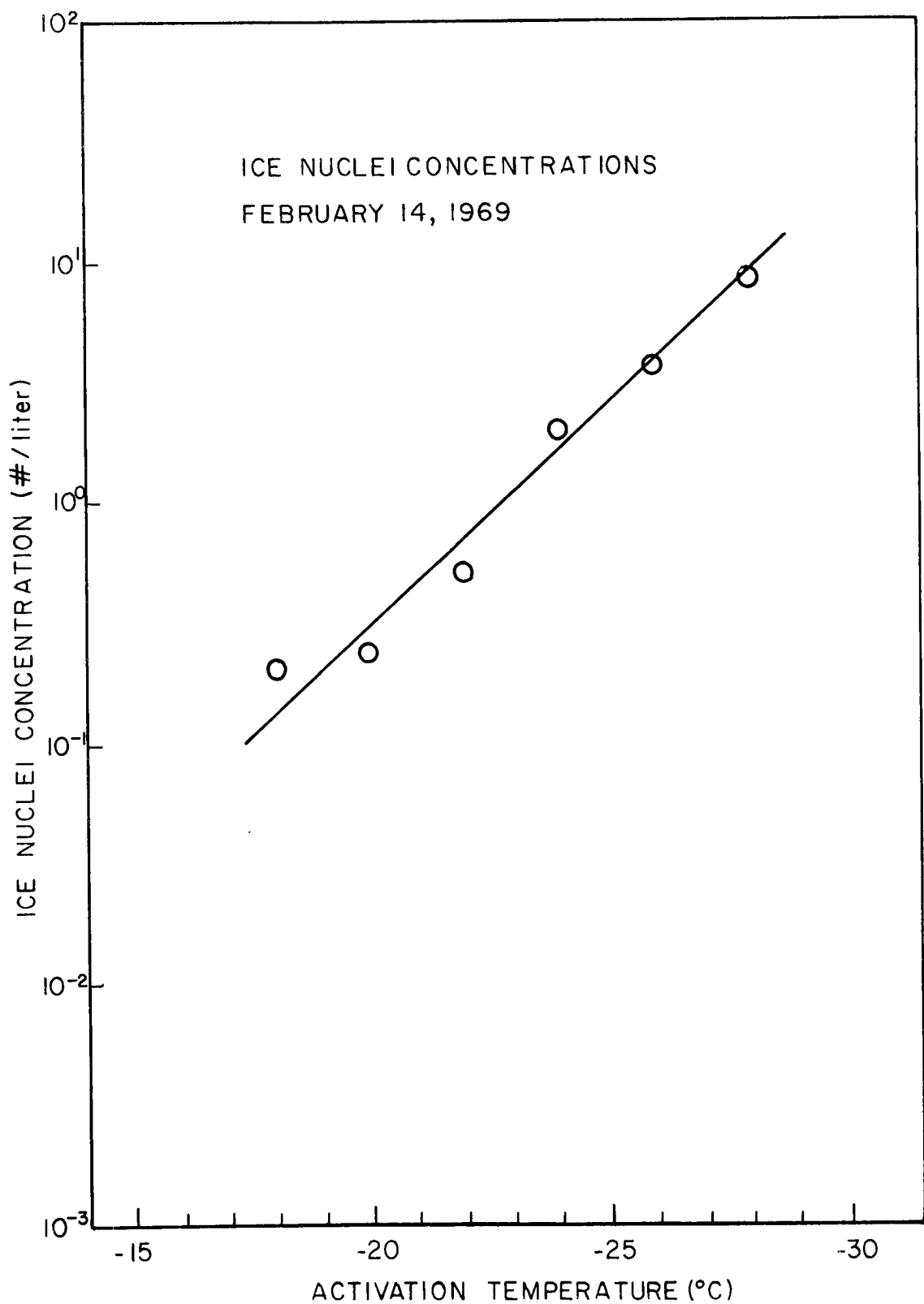


Fig. D12 Ice-Nuclei Spectrum for February 14, 1969

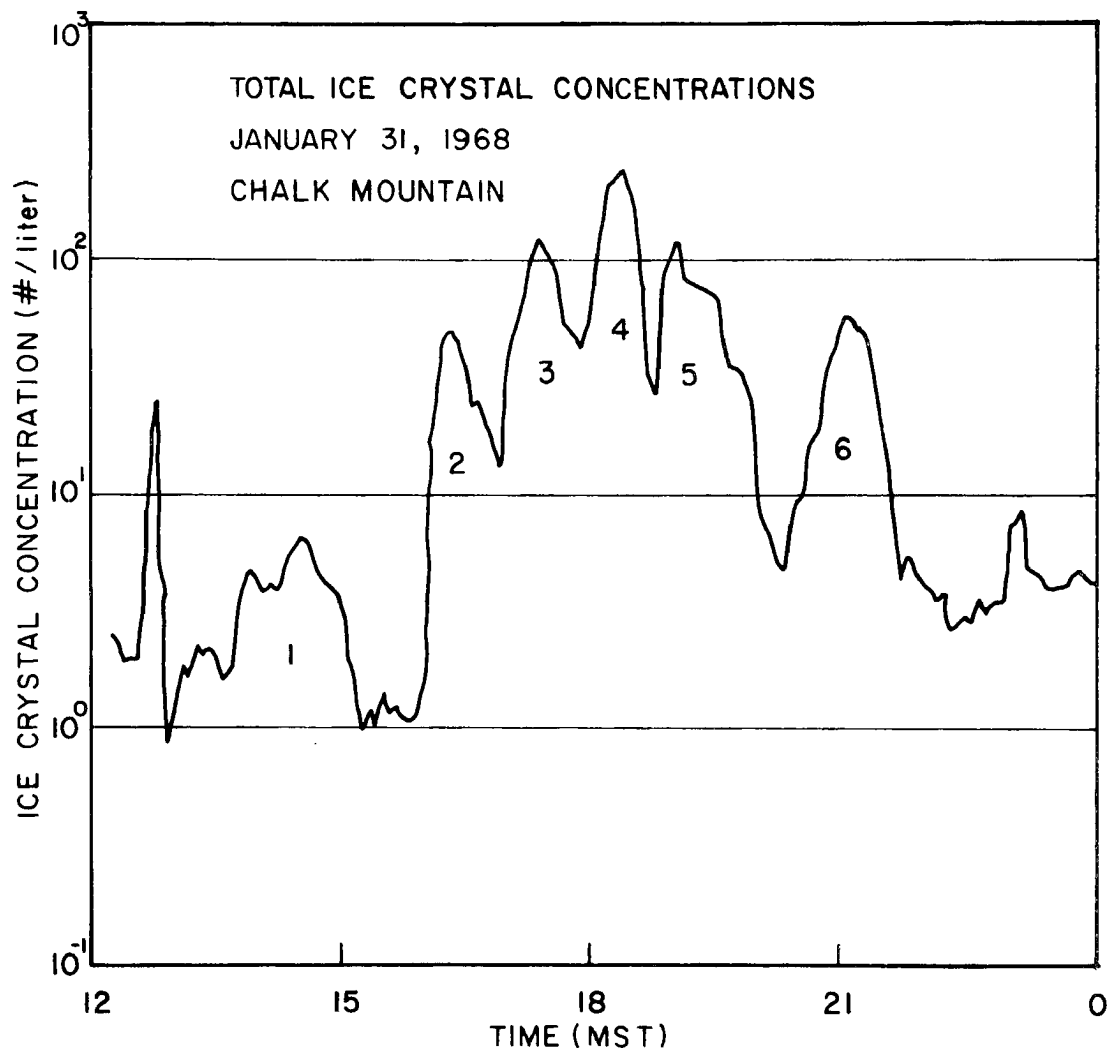


Fig. D13 Ice-Crystal Variation with Time for January 31, 1968

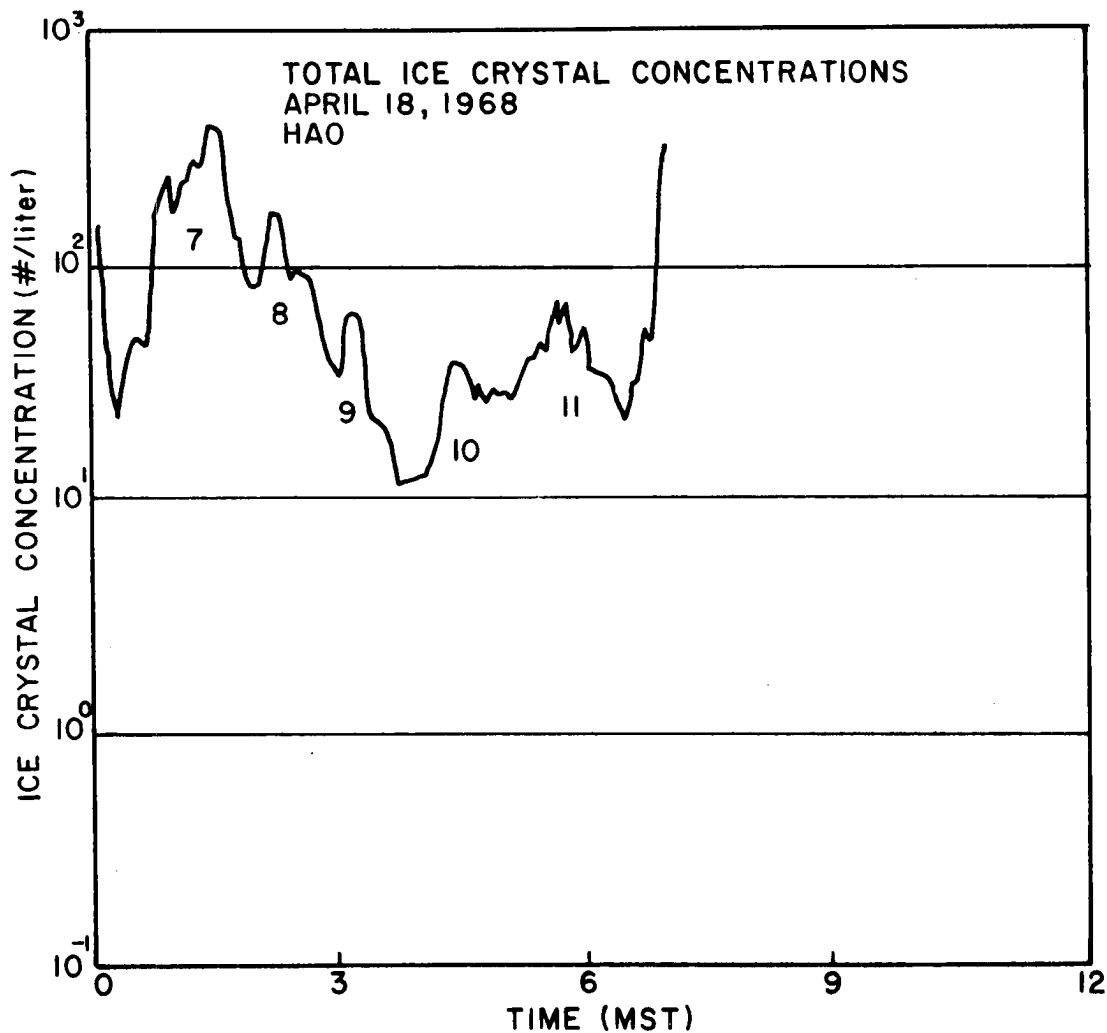


Fig. D14 Ice-Crystal Variation with Time for April 18, 1968

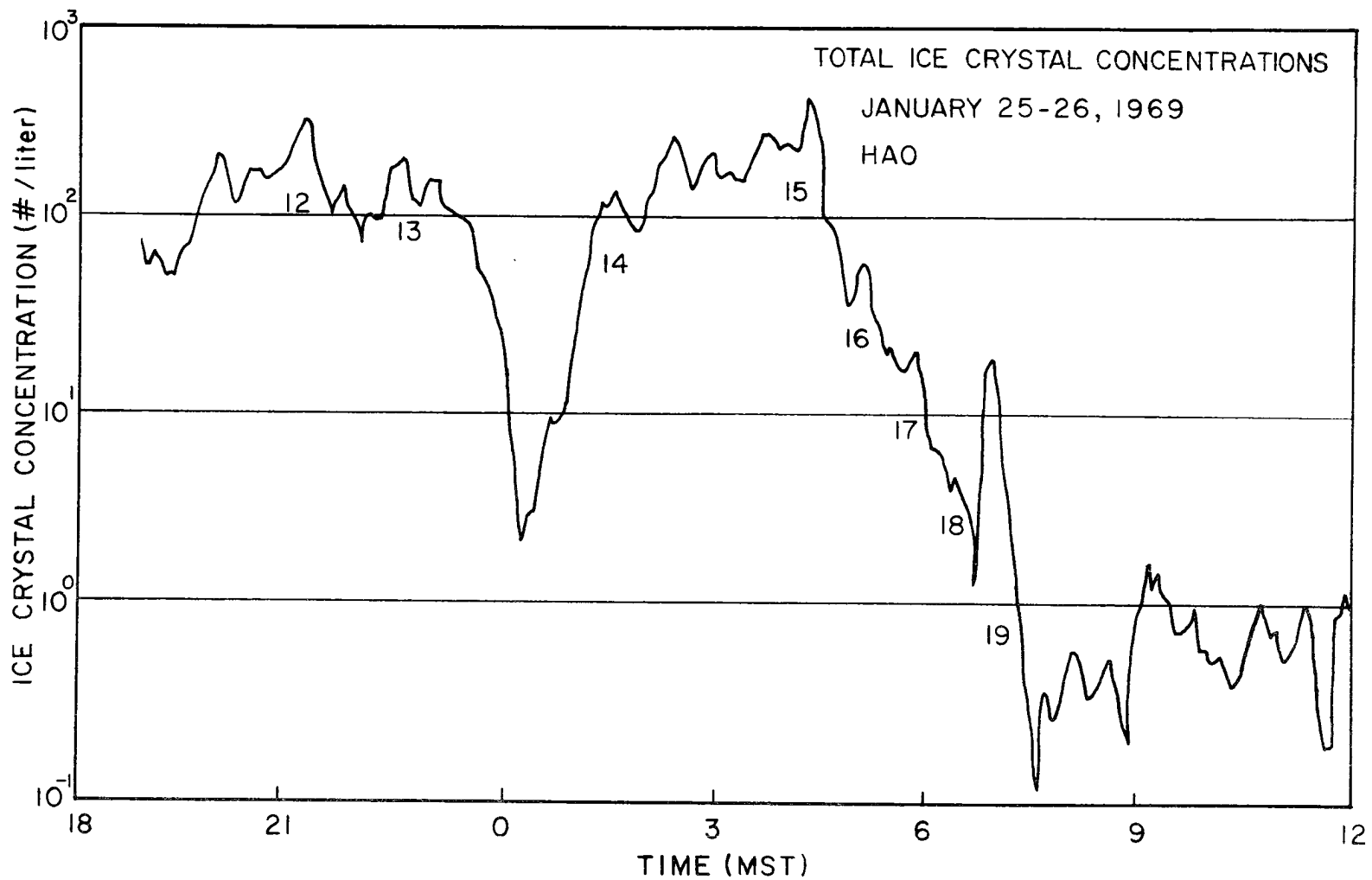


Fig. D15 Ice-Crystal Variation with Time for January 25, 1969

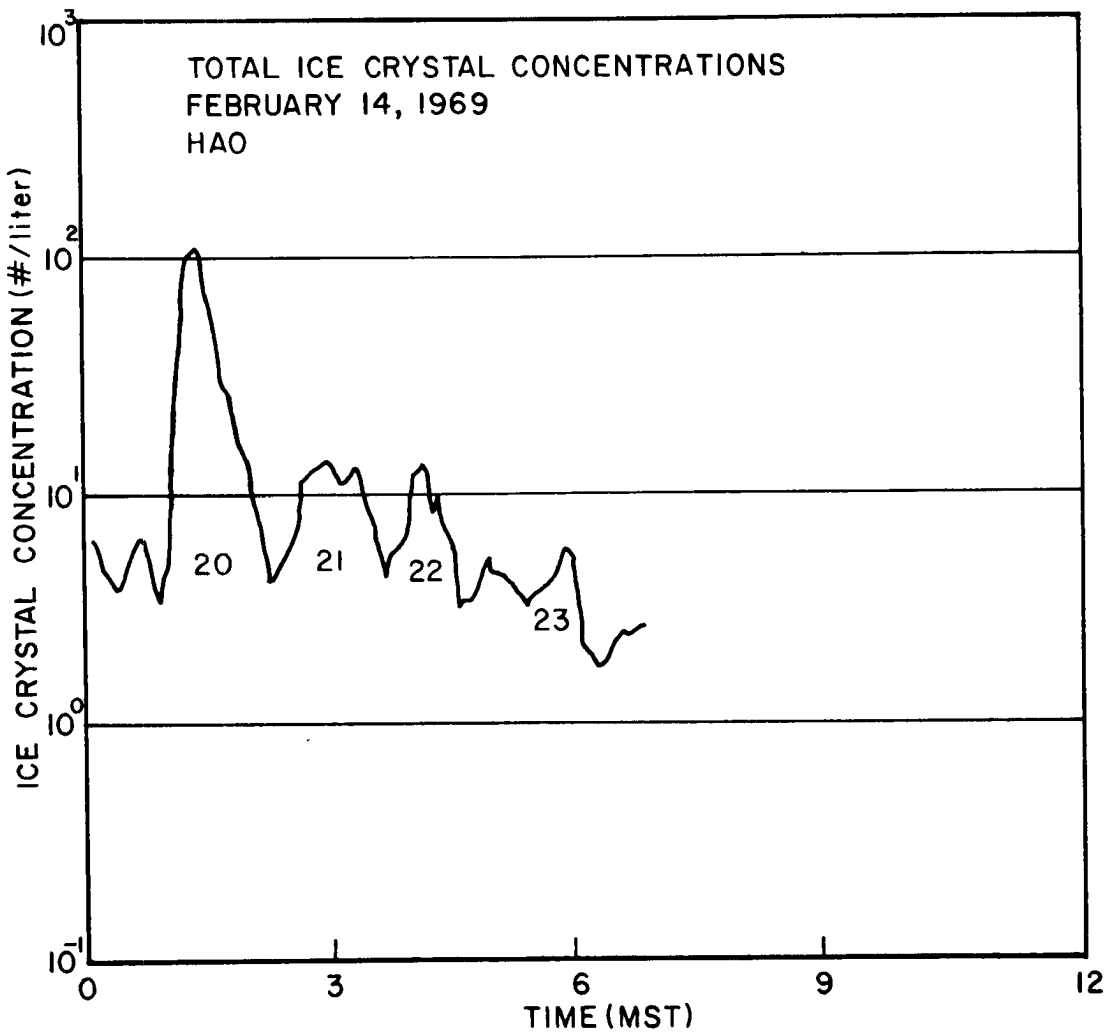


Fig. D16 Ice-Crystal Variation with Time for February 14, 1969